ALMA MATER STUDIORUM – UNIVERISTÁ DI BOLOGNA

DOTTORATO DI RICERCA IN SCIENZE BIOCHIMICHE E BIOTECNOLOGICHE

CICLO XXVII

Settore concorsuale: 05 / E1

Settore scientifico – Disciplinare: BIO12

Role of Magnesium and its mitochondrial transporter MRS2 in the modulation of drug-induced apoptosis leading to multidrug resistance phenotype

Presentata da: Lucia Merolle

Coordinatore dottorato
Prof. Santi Mario Spampinato

Relatore:
Prof. Stefano Iotti

Esame finale anno 2015

Table of Contents

1 MAGNESIUM

1.1 Introduction

Magnesium (Mg) probably derives its name from Magnesia, *Μάγνήσιά* , which is a prefecture in Thessaly, Greece were it was first found and to this present day a lot of magnesium ore is present in the area.[1,2] The first evidence of Mg in the history of medicine dates back to 1695 when N. Grew separated the solid salt Magnesium Sulfate from the Epsom spring water. This latter was a commonly used remedy in the 16th century known for its healing properties. [3]

Later on, in 1755 Joseph Black recognized Mg as an element and after about fifty years Sir Humphrey Davy isolated pure magnesium.[4]

Classified as alkaline earth element, Mg has an atomic number of 12 and is present in three stable isotopes ^{24}Mg, ^{25}Mg, ^{26}Mg but we usually refer to the ^{24}Mg, which is the most common isotope with a percentage of 78.99%.[1,5]

Mg^{2+} , which virtually always exhibits a +2 oxidation state because of the loss or sharing of its two 3s electrons, is the 8th most abundant element in the earth in the form of solid salts; furthermore, it is the most abundant divalent cation in the cells. Since many magnesium salts are highly soluble in water, this cation presents a high bioavailability for the cells. Due to its unique physical and chemical properties and its abundance in the intracellular environment, Mg^{2+} participates in a host of biological processes and can be ascribed to the so-called essential elements for human life.[6,7] The National Institute of Health recommend a daily Mg^{2+} intake of 420 mg for men and 320 mg for women.[8] Indeed, Mg^{2+} deficiency has been associated with a wide range of diseases including diabetes mellitus type 2, hypertension, migraine and depression. [5,9,10]

1.2 Magnesium ion channels and transporters

The majority of eukaryotic cells tend to ensure that the magnesium concentration in the cell remains unchanged even when a major trans-membrane gradient is artificially imposed. For example, different hormones are able to induce the movement of large amounts of total Mg^{2+} in either directions across eukaryotic cells membranes whereas relatively slight variations occur in free intracellular Mg^{2+}.[11,12,13] This indicates the ability of the cell to tightly regulate intracellular Mg^{2+} content by precise control mechanisms at the level of entry, efflux, intracellular buffering and compartmentalization. Although these Mg^{2+} intracellular variations are small, they could alter Mg^{2+} levels in cell organelles profoundly influencing signalling pathways that regulate cellular functions.[14,15,16] Mitochondria are the most affected organelles with important repercussions on cellular bioenergetics.[17]

As previously stated, Mg^{2+} deficiency was found to be associated to several diseases such as hypertension, eclampsia and cystic fibrosis. Therefore, the regulation of cellular Mg^{2+} homeostasis is critical for numerous cellular functions and has high clinical relevance.[18]

Being the second most abundant cellular divalent cation, Mg^{2+} handling in the cell is usually maintained in the range of 10-30 mM. However, since most of the intracellular Mg^{2+} is bound to macromolecules the concentrations of freely available Mg^{2+} falls within the low millimolar range 0.2-1.2 mM.[19,20] Mg^{2+} intracellular levels are regulated by the activity of many powerful cations transporters localized in the cell membrane surface as well as in the membrane of cellular organelles.[17] Amongst cellular organelles mitochondria represent the major Mg^{2+} intracellular pools.[21,22] Circumstantial evidences, suggest that Mg^{2+} can be mobilized from mitochondria under various conditions including

hormonal stimuli and that part of the observed variations in mitochondrial magnesium is related to the control of respiration.[15,23,24]

Magnesium transport can be driven by channels, which allow accumulation, or exchange mechanisms, which allow extrusion.[17,25] Table I reports the main Mg^{2+} transporters in eukaryotic cells.

Aside the two mechanisms favouring the entry of Mg^{2+} into mitochondria and Golgi, all the other influx transporters are located at the cell membrane level. Channels allowing Mg^{2+} entry into the cell were firstly described for prokaryotes and protozoan.[26,27,28] Only recently, several Mg^{2+} entry mechanisms with channels or channels-like features have been identified in eukaryotic cells.

Table I **Magnesium transporters in mammalian cells** (table adapted from J.de Baaij 2015 and A.Romani 2011)[5,25]

Mg^{2+} Transporters					
Cell localization	**Protein Family**	**Members**	**Expression**	**Permeability**	**Mechanism**
Influx mechanism					
Mitochondria memebrane	MRS2	Mrs2/AtMrs2,Lpe10	Ubiquitous	Mg>Ni	Channel
Golgi	MMgT	MMgT1			Channel
		MMgT2			
Plasma membrane	TRPM	TRPM6	Kidney, Intestine	Ba>Ni>Mg>Ca	Channel
		TRPM7	Ubiquitous	Ba>Ni>Mg>Ca	Channel
	Claudins	CLDN16	Kidney		Channels
		CLDN19			
	MagT1	MagT1	Ubiquitous	Mg>Ba>FE=Cu	Channel
	MgTE	SLC41A1	Ubiquitous	Mg>Sr>Fe>Ba>Cu	Exchanger
		SLC41A2		\	Exchanger
		SLC41A3			
	CNNM	CNNM1	Brain	Cu>Mg?	?
		CNNM2	Kidney	Mg>Sr>Zn>Cd	Transporter?
		CNNM3	Ubiquitous	Mg>Fe>Cu>Co	Transporter?
		CNNM4	Intestine	Mg	Exchanger?
Efflux mechanism					
	Na^{+}/Mg^{2+} exchanger				Antiport
	Na-indipendent				Exchanger
	H^{+}/Mg exchanger				Exchanger
	Mn^{2+}/Mg^{2+} antiporter				Exchanger
	Ca^{2+}/Mg^{2+} antiporter				Exchanger

Before listing the main Mg^{2+} transporters, it is worth mentioning the peculiarity of the ionic radius of Mg^{2+} and its coordination geometry.[1,29] Mg^{2+} has the largest radius of all cations when hydrated, but is among the smallest when dehydrated with a 400-fold increase in volume.[30] Moreover, the Mg^{2+} ion is almost invariably hexacoordinated and maintains strict bond lengths and bond angles (2.15+-0.1A and 90° respectively). It also binds the hydrating waters stronger than other cations like sodium, potassium and calcium; this feature leading to the postulation that activity of magnesium as an enzyme cofactor is mediated through spatial coordination of bound water molecules. These peculiar properties pinpoint the special role of Mg^{2+} in catalysis, biological

structures and regulation of many cellular processes and must be taken into account when studying the binding of Mg^{2+} to cellular macromolecules.[31] In the case of macromolecules such as transport proteins, these have to be able to recognize the hydrated cation and then to remove the hydration shell to let Mg^{2+} pass through membrane.[1] Consequently, this mechanism of transport requires a lot of energy.[5] Taking all together, these unique features of magnesium lead us to believe that the system for magnesium transport should be rather unique too.[32]

1.2.1 Exchange mechansims

Mg^{2+} extrusion is operate by two kind of exchange mechanisms: the Na^+-dependent and the Na^+-independent pathways, but information about their operation, abundance and tissue specificity remains largely unknown.[17]

The main mechanism, originally proposed by Theodor Gunther in 1984, is currently believed to be a Na^+-dependent Mg^{2+} efflux. This notion has been supported by a large body of evidence in literature and characterized in many cell types. Though the stoichiometry of this exchange is not fully elucidated, it has been found that its activation is mediated by cAMP. Indeed, stimulation of β-adrenergic, glucagon or administration of forskolin all results in Mg^{2+} extrusion via cAMP mediated phosphorylation of the Na^+-dependent mechanism. [33,34]

Nevertheless, in the absence of extracellular Na^+ to support the Na^+/Mg^{2+} exchanger a Na^+-independent Mg^{2+} extrusion pathway has also been shown to exist. Although it remains poorly characterized it seems that different cations including Ca^{2+} or Mn^{2+} or anions such as HCO_3^- or Cl^- are utilized by this mechanism. However it remains unclear whether it operates as antiporter for cations or sinporter for cations and anions.[35]

1.2.2 CorA family proteins

CorA proteins is a group of ion transporters that mediate transport of divalent metal ions across biological membranes.

CorA proteins are abundant among the prokaryotic organisms but homologues are present in both human and yeast. The activity of CorA proteins has generally been associated with the transport of magnesium ions but the members of this family can also transport other ions such as cobalt and nickel.[32]

This family of proteins present two predicted transmembrane domains, separated by short loop-oriented to the outside of the membrane and a YGMN/F motif at the end of the N-terminus.[18]

The functional homologues characterized in the inner mitochondrial membrane of yeast and mammals are the MRS2/LPE10 type, and in the plasma membrane of yeast the ALR/MNR type.[36,37]

1.2.2.1 MRS2

Whereas CorA proteins mediates Mg^{2+} influx in most of the prokaryotes, MRS2 family channels deal magnesium transport in mammals and are the only recognized Mg^{2+} transporter in mitochondria of mammals, yeast and plants.[38] In eukaryotes, the CorA-like Mrs2 protein was firstly characterized in *Saccharomyces cerevisiae* mitochondria by a genetic screening affecting splicing of group II introns.[39]

Mrs2 is a pentameric protein resembling a funnel of ~50 kDa nuclear encoded (Fig. 1) which shares with CorA superfamily proteins the two TM domain and the glycine–methionine–asparagine (GMN) motif which is essential for channel function.[40] The CorA-like Mrs2 protein, found to localize in mitochondrial inner membranes is required for normal mitochondrial Mg^{2+} homeostasis and

function, the stability of mitochondrial respiratory complexes and the maintenance of myelination within the central nervous system.[41,42] Notably, Mrs2 expression is a genetic hallmark of embryonic stem cells.[43] Although ion selectivity remains unclear despite numerous studies, the conserved GMN sequence motif at the end of TM1 α-helix on the outer surface of the membrane is considered to be essential for Mg^{2+} recognition.[40,44]

Mrs2 forms a Mg^{2+} selective, high-conductance channel which controls Mg^{2+} influx into mitochondria. The motor of this *Mg^{2+}-influx pathway* appears to be the mitochondrial membrane potential $\Delta\psi_m$. Accordingly, pharmacological agents inhibiting the F1-F0 ATP synthase or the ADP/ATP translocase are able to modulate Mrs2 activity leading to a substantial decrease of the amplitude Mg^{2+} influx. An elegant experiment conducted on isolated yeast mitochondria by *Kolisek et al.* shows how Mrs2 overexpression induces a marked increase in free mitochondrial magnesium, while the deletion of the gene abolishes this high capacity influx.[42] Evidence for the contribution of Mrs2 protein in mitochondrial Mg^{2+} uptake also come by the fact that knockdown of the gene results in functional defects of mitochondria, decrease of mitochondrial Mg^{2+} and defect in RNA splicing. Moreover, expression of the bacterial CorA protein in yeast and targeted to the mitochondria, could partially compensate for these mutant effects by restoring wild-type levels of mitochondrial magnesium.[41]

In human, the gene codifying for the active protein MRS2, is located on chromosome 6 and is composed of 11 exons, after translation the protein is transported to the inner mitochondrial membrane.[45]

In human, it has also been demonstrated that the presence of MRS2 protein is necessary for human cell survival. In 2009 *Piskacek et al.* reported that knocking down MRS2 channel in human embryonic kidney (HEK-293) cells impairs the expression of the mitochondrial complex I of the respiratory chain, reduces the level of mitochondrial Mg^{2+}, affects cell morphology and promotes apoptosis. It

was shown that all these concomitant effects lead to the loss of cell viability within 2 weeks.[46] It is unclear whether the decrease in mitochondrial Mg^{2+} depends on the absence of MRS2 or is due to the complex I depletion, which affects mitochondrial membrane potential $\Delta\psi_m$ and the consequently Mg^{2+} retention within the organelle.

MRS2 expression has also been associated to drug resistance of gastric cancer cells. *Chen et al.* observed an up-regulation of this channel in doxorubicin resistant cells respect to the sensitive counterparts.[47] Furthermore, they demonstrated that transfection with MRS2 in wild type cells confers *Multi Drug Resistance* (MDR) phenotype; conversely, knocking down the MRS2 partially reverse the acquired resistance.[45] These results suggest a direct correlation between MDR phenotype and MRS2 expression.

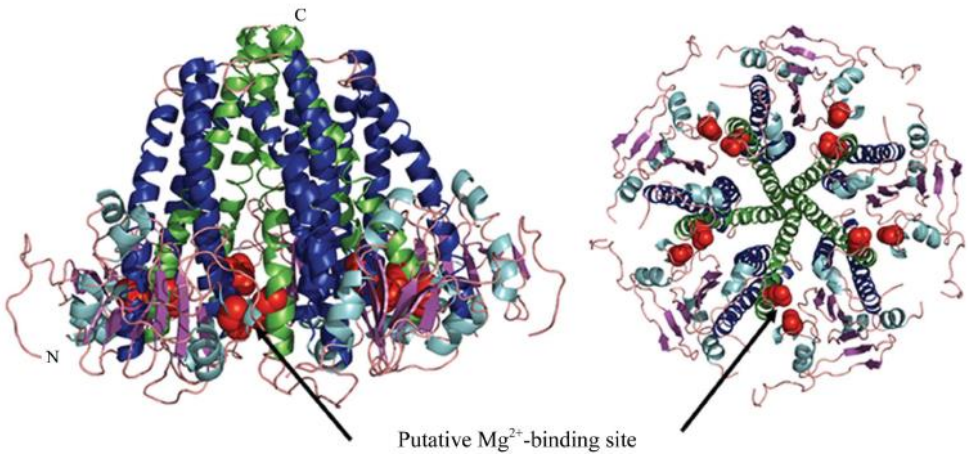

Figure 1 Model of the yeast (*Saccharomyces cerevisiae*) Mrs2 protein. The channel is assembled as a homopentamer resembling a funnel. The putative Mg^{2+}-binding site is mapped in reds.[40]

1.2.3 TRPM channels

The transient receptor potential (TRP) ion channel family plays critical roles in mediating cellular responses to a wide range of physiological stimuli. This family of proteins is divided into six related sub family proteins, including the TRPM sub family members.[48]

The melastatin-related TRP family (TRPM) is divided, in its turn, into four groups: TRPM1/3, TRPM2/8, TRPM4/5 and TRPM6/7.

TRPM6 and TRPM7 were the first Mg^{2+} channels identified in mammalian cells by different approaches. Both proteins share the unique feature of an atypical kinase domain at their C-terminus for which they have been termed '*chanzymes*' (*chan*nels plus en*zymes*). TRPM6 has also the faculty to phosphorylate residues of TRPM7 channel forming heterodimeric complexes as well as homodimeric complexes with itself. The two channels plus the heterodimeric complex are distinct ion channel exhibiting different divalent cation permeability, pH sensitivity and unique single channel conductance.[2516,17]

TRMP6 is specifically located in the colon and in the distal convolute tubule of the nephron. This distribution strongly emphasizes the role of this channel in controlling whole body Mg^{2+} homeostasis via intestinal absorption and renal re-sorption. Indeed, kidney is the principal organ involved in magnesium homeostasis. However, it is unresolved how Mg^{2+} accumulated in the apical domain of the tissue can be transported across the cytoplasm, delivered to the basolateral domain and be extruded into the blood plasma. One hypothesis is that baso-lateral Mg^{2+} extrusion occurs via Na^{+}/Mg^{2+} exchanger. Impairment of TRPM6 expression has been associate to a genetic form of hypomagnesemia accompanied by hypocalcemia poorly restored by massive Mg^{2+} administration.[17,49]

TRPM7 is an ubiquitous channel founded in every mammalian tissue investigated to date. The TRPM7 channel was suggested to provide a major mechanism of Mg^{2+} entry into the cell, thus regulating both cellular and whole body Mg^{2+} homeostasis. [50]

The TRPM7 channel involvement in cellular Mg^{2+} homeostasis was demonstrated by genetic knockout experiments. This genetic manipulation led to an arrest of cell proliferation and reduced Mg^{2+} levels that could be restored exclusively by Mg^{2+} supplementation, suggesting that the major role of TRPM7 is regulating Mg^{2+} intake. [50,51] Besides, TRPM7 activity is often regarded as a requirement for cell survival since genetic or pharmacological ablation led to an arrest in G0/G1 of cell cycle and genetic ablation of TRPM7 induce apoptosis of mast cells.[50] All these data are consistent with the fact that proliferating cells require Mg^{2+}.

Regulation of TRPM7 depends on cytosolic availability of Mg^{2+} and Mg^{2+}-ATP^{2-}. Activation of TRPM7 only occurs in the presence of physiological Mg^{2+} within the cell. However TRPM7 is not an exclusive Mg^{2+} channel being able to also transport other cations such as Ca^{2+} or Zn^{2+}.[17]

Despite the mounting evidence for TRPM7 as a regulator of Mg^{2+} homeostasis, recently has been published that TRPM7-deficient mouse showed altered embryonic development and disrupted thymopoiesis without affecting total intracellular Mg^{2+} concentration of T cells.[5]

Concluding, TRPM7 is involved in a number of vital cellular processes in mammalian cells, and has gaining increasing attention for its potential role in cancers as a new diagnostic and prognostic marker, in addition to known biomarkers.[52]

1.2.4 Claudins

Claudin-16 was the first Mg^{2+} transporter to be identified in mammalian cells. Mutation of this protein results in the Familial Hypomagnesaemia with Hypercalciuria and Nephrocalcinosis (FHHNC) which is a is a genetic disease characterized by Ca^{2+} and Mg^{2+} wasting. This protein mediates paracellular Ca^{2+} and Mg^{2+} fluxes throughout the nephron. However, the modality by which these fluxes are generated is still controversial. CLND16 is a member of the claudin family, which are tight junction proteins with 4 trans-membrane spans coordinated by 2 extracellular loops, and with both C- and N-termini on the cytoplasm side.[53]

Recently another claudin isoform has been shown to be involved in the reabsorption of Mg^{2+} and Ca^{2+} : Claudin-19. This protein forms a heteromeric complex with claudin-16 at the level of the tight junction, with specific cation-selectivity. Point mutation of both of these proteins affects the heteromeric interaction leading to development of FHHNC.[5]

1.2.5 MagT1

Mg^{2+} transporter 1 (MagT1) is an ubiquitously expressed Mg^{2+} channel. Although the identification of this channel dates back almost 10 years, the functional characteristics of MagT1 are still undetermined. The most available hypothesis is that MagT1 has similar function on TRPM7 in certain types of cells. In particular, it mediates rapid Mg^{2+} entry in T cells upon receptor activation.[54] This hypothesis is also supported by the fact that overexpression of MagT1 can partially rescue cell growth and Mg^{2+} uptake in TRPM7-deficient cells.[55]

1.2.6 SLC41

Members of the Solute Carrier family 41 are found in all eukaryotic cells and show distant homology to the prokaryotes Mg^{2+} transporter MgtE. This family channel was first identified and characterized in 2003 and comprehend three family members: SLC41A1, SLC41A2 and SLC41A3.[56]

SLC41A1 is the most extensively studied channel of his family thought to mediate Mg^{2+} transport across the plasma membrane, whereas SLC41A2 might be involved in the subcellular Mg^{2+} transport. Recently, has been found that the expression of SLC41A1 in HEK-293 cells leads to Mg^{2+} efflux, thus it has been proposed that this protein may function as Na^{+}/Mg^{2+} exchanger with a 2:1 stoichiometry.[57] It seems that single nucleotide-polymorphisms (SNPs) of SLC41A1 have an impacts on neurodegenerative diseases, in particular with Parkinson's disease.[58]

1.2.7 CNNM

Members of the Cyclin M proteins, also known as ACDP family, have been proposed to function as Mg^{2+} transporters. These proteins present more than 50% of homology with the CorC transporter which is implicated in Mg^{2+} efflux in prokaryotes. CNNM1 is essentially restricted to the brain, CNNM2 expression is high in kidney and CNNM4 is mostly expressed in intestine. On the contrary, CNNM3 is an ubiquitous channel and may play a role in the maintenance of cellular Mg^{2+} homeostasis. Furthermore this transporter seems to be involved in cancer. In particular, it has been found that CNNM3 activity is regulated by the oncogene PRL2 and that his interaction could be essential for Mg^{2+} influx that drives tumour progression. [59]

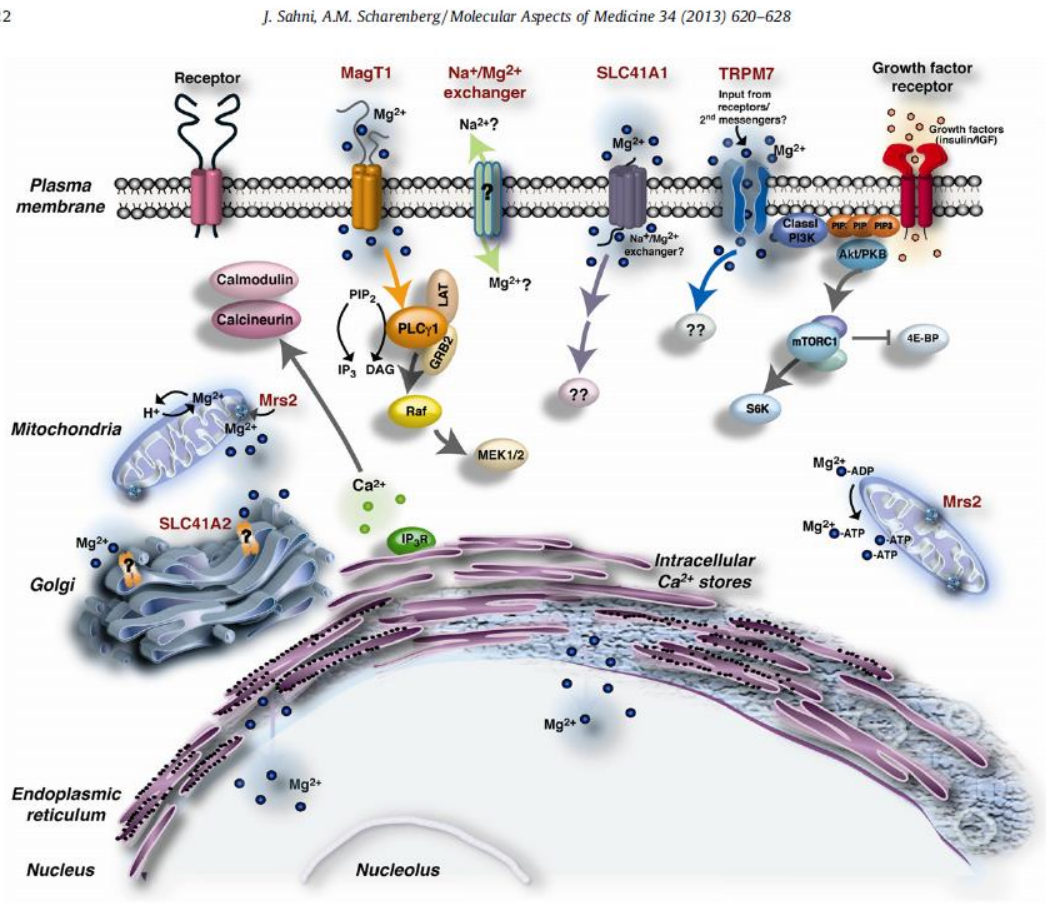

Figure 2 Magnesium regulation by its transporters in vertebrate cells . The cartoon summarizes the combined action of Na^+/Mg^{2+} exchanger, TRPM7, SLC41A1, Mag T1, and MRS2 Mg^{2+} transporters as well as the main cellular functions regulated by changes in Mg^{2+} content within different compartments.[56]

1.3 Regulation of Magnesium transport and homeostasis

Over the last 20 years, the elucidation of the complex mechanism underlying Mg^{2+} transport across cellular membranes has been object of deep research. In particular, Mg^{2+} transporters are finely regulated by different metabolic stimuli such as hormonal and pharmacological factors including β-agonists, growth factors, and insulin. It has been suggested that a hormonally regulated magnesium uptake system controls intracellular magnesium concentration in cellular compartments. The magnesium concentration in these compartments would then serve to regulate the activity of magnesium-sensitive enzymes.[60]

Extrusion. Mg^{2+} extrusion, is mainly regulated by hormones such as catecholamine or glucagon. These hormones, known to increase cellular cAMP level by activating G-protein coupled receptors, are able to induce a rapid Mg^{2+} efflux by the activity of Na^{+}/Mg^{2+} exchangers. Indeed, it has been shown that many different type of cells respond with a massive Mg^{2+} efflux returning to baseline levels within 8 minutes from the application of the stimulus. This temporally limited extrusion suggest that Mg^{2+} can be mobilized from a well-defined cellular pool. The key role of cAMP mediated extrusion is further corroborated by the observation that pre-treatment of cells with hormones or agents that decrease cAMP levels, are able to prevent cellular Mg^{2+} mobilization.[61,62]

However, cAMP independent Mg^{2+} extrusion mechanisms associated with α_1-adrenergic stimulation, have also been reported.[63] In particular, administration of phenylephrine promotes Mg^{2+} extrusion from liver cells depending on the activation of capacitive Ca^{2+} entry. Hence, it would appear that an optimal level of cytosolic Ca^{2+} has to be reached in order to elicit Mg^{2+} extrusion. This mechanism evidences the crosstalk with Ca^{2+} signalling and Mg^{2+} homeostasis.

Mg^{2+} extrusion can also occur in condition of low ATP levels within the cell.

Indeed, cells exposure to agents or conditions decreasing ATP levels by several mechanisms, such as preventing the mitochondrial electron chain[15] or acting as an ATP trap[64], affects Mg^{2+} homeostasis. The impairment of Mg^{2+} can be attributed to the Mg^{2+}-buffering role elicited from ATP within the cell. Indeed a decrease of ATP or its degradation in ADP or AMP results in an increase of free cytosolic Mg^{2+} which ultimately originates its extrusion from the cells.

Accumulation. Although the regulation mechanism concerning Mg^{2+} extrusion are well known, information about structural details are still lacking. On the contrary, in the case of Mg^{2+} entry we have a lot of structural information about

channels and transporters but we need more information about how they are regulated.

The main pathway for Mg^{2+} accumulation in mammalian cells is the activation of protein kinase C (PKC). Evidence supporting role for PKC in mediating Mg^{2+} accumulation has been provided by several laboratories.[65] Furthermore, inhibition of Mg^{2+} accumulation has been observed following treatment of cells with the PKC inhibitor staurosporine. [66]

However, other pathways are involved in the regulation of Mg^{2+} entry such as MAPKs and EGF signalling. [67] It has been shown that the inhibition of MAPKs signalling impedes Mg^{2+} entry and block cell cycle progression by affecting cyclin activity while EGF controls the TRPM6 channel expression and consequently Mg^{2+} reabsorption in kidney.[68]

1.3.1 Perturbation of magnesium homeostasis

Perturbation of Mg^{2+} homeostasis may result in impairment of electrochemical and electrolytic balance causing dysfunction of several tissues and organs.

Serum magnesium levels above 1.1 mM are generally considered hypermagnesemia. The main symptoms of hypermagnesemia are nausea, vomiting, headaches or flushing. When Mg^{2+} arise above 3.0 mM it can lead to serious cardiac defects that are characterized by bradycardia or hypotension ultimately leading to coma, asystole or cardiac arrest. Fortunately, hypermagnesemia is rare, whereas hypomagnesemia is significantly more prevalent.

Hypomagnesaemia, is defined as any serum concentration of magnesium under 0.74 mM. Patients affected by hypomagnesaemia suffer from nonspecific symptoms such as depression, tiredness, muscle spasms and muscle weakness.

Diagnosis may take years, due to the absence of a routinely determination of serum Mg^{2+} level in patients[5]

In general, the main causes of hypomagnesaemia are the following: chronic inadequate Mg^{2+} intake exacerbate by vomiting and diarrhoea; alcoholism caused by the block of Mg^{2+} uptake from ethanol.[69,70] However there are also genetic causes of hypomagnesaemia often associated with deregulation of magnesium transporters. The most common genetic cause of isolated hypomagnesaemia are mutation in CLDN16 and TRPM6 channels. Mutation of CDLN16 causes Ca^{2+} and Mg^{2+} wasting, renal parenchymal calcification and renal failure. In this pathological condition Mg^{2+}supplementation is not capable to restore normal serum Mg^{2+} levels or retarding disease progression.[53] Moreover, mutation in TRPM6 channel causes hypomagnesaemia with secondary hypocalcaemia resulting in severe neurological complications such as epilepsy and mental retardation.[49] Similar defects are associated with mutation of CNNM2 channel, causative for hypomagnesaemia with Mg^{2+} serum levels range between 0.3 and 0.5 mM.[71]

One of the most common side effects of chemotherapy and radiotherapy, especially in the treatment of tumours with cisplatin or when used in combination with anthracyclines or 5-fluorouracil is serum magnesium deficiency. The hypomagnesaemia induced by cisplatin is a consequence of the nephrotoxicity of this drug, causing tubular damage and consequently general electrolyte wasting.

Syndromes of magnesium deficiency has also been observed in patients treated with the anti-epidermal growth factor (EGFR) IgG1 monoclonal antibody, cetuximab. It seems that cetuximab causes an inhibition of Mg^{2+} reabsorption in the renal distant convolute tubule, without affecting function or morphology of nephrons. TRPM6 channel is also involved as it is responsible for Mg^{2+} absorption in the intestine and kidney. *Groenestage et al* defined EGF as

magneisotropic hormones regulating renal Mg^{2+} reabsorption by controlling the activity of TRPM6.[72] As a consequence, inhibition of the EGFR by anti-EGFR antibodies such as cetuximab, lead to suppression of TRPM6 activity and renal Mg^{2+} wasting.

1.4 Magnesium in Cell Biochemistry

In 1927 Erdtman discovered the involvement of Mg^{2+} as activator of mammalian alkaline phosphatase [73] and since then a multitude of enzymes have been shown to be activated by this cation. Scientific literature reports a number of 300 enzymatic reactions in which Mg^{2+} is involved, however this is an approximation largely underestimating the real figure. Currently, enzymatic databases list over 600 enzymes for which Mg^{2+} acts as a cofactor and other 200 in which may act as direct activator.5 In particular, Mg^{2+} is implicated in those reactions utilizing ATP or catalyzing the transfer of phosphate. Indeed ATP hydrolysis to ADP is the most significative role of Mg^{2+} in energy metabolism and it is a matter of fact that all reactions involving ATP need the presence of Mg^{2+} ions as the functional ATP form is $MgATP^{2-}$.[74] Since ATP is essential for almost all of the biological processes that require energy, including oxidative phosphorylation, nucleic acid synthesis, protein synthesis and so on, the function of magnesium can be extended to all of those enzymatic reactions.[75] Mg^{2+} bounded to ATP is also needed in those reactions necessitating phosphate group transfer such as glukokinase, phohphofructokinase, phoshoglyceratekinase and pyruvatekinase.[76] Consequently, Mg^{2+} availability is of major importance for glucose metabolism. Mg^{2+} can act as a cofactor in three ways: by stabilizing a reaction intermediate, ii) by stabilizing a product leaving group; iii) by binding two reactive substrates simultaneously and facilitating a

reaction trough a proximity effect. In addition Mg^{2+} can also bind directly to enzymes, thereby modifying enzyme structure or acquiring a catalytic role.[77]

Mg^{2+} ion is an essential component of the RNA and DNA tertiary structures, as it binds the negatively charged O and N molecules within the polynucleotide chain. It has been observed that in Mg^{2+} deficient conditions, DNA is more accessible to free oxygen radicals and more prone to oxidative stress. On the other hand, higher Mg^{2+} concentration could deforming the double helix conformation. Hence, maintaining cellular Mg^{2+} concentration within the physiological range is essential for DNA stability.[78] It has been found that DNA polymerases have two Mg^{2+} binding sites, hereby Mg^{2+} in necessary for the structure of DNA and RNA polymerases; moreover, the release of Mg^{2+} ions is necessary for the opening of the catalytic site for new nucleotides.

Finally, the presence of Mg^{2+} is also important for the maintaining of genomic stability through ensuring the fidelity of DNA replication and repair processes.[79]

1.4.1 Magnesium in Cell Signalling

Mg^{2+} acts as a physiological Ca^{2+} antagonist within cells, and as a result, the Mg^{2+}/Ca^{2+} ratio is of major importance for the activity of Ca^{2+}-ATPases and other calcium transporting proteins. Small changes in the Mg^{2+} availability within the cell may therefore cause disturbed calcium signalling or toxicity related to it.[80] Moreover, a second messenger role for Mg^{2+} has been proposed when Mg^{2+} efflux was determined following insulin exposure. Recently, in a study on T-cell activation, MagT1 channels were shown to mediate Mg^{2+} influx upon T-cell receptor activation and EGF stimulation. In these cells, Mg^{2+} activates phospholipase C- (PLC), resulting in reduced phosphorylation of protein kinase

C (PKC) and inositol triphosphate (IP3) generation downstream, eventually leading to reduced Ca^{2+} influx. In contrast, other reports that PLC activation precedes Mg^{2+} influx. Prosecuting studies demonstrated that MagT1-deficient cells have severely reduced basal intracellular Mg^{2+} concentrations, suggesting that the effects seen on PLC are dependent on general intracellular Mg^{2+} availability.[81]

1.4.2 Magnesium and Cell Proliferation

Since 1980s several investigators described the essential role of Mg^{2+} in the proliferation of yeast and mammalian cells. Mg^{2+} might reasonably be involved in every single step of the mitogenic signalling cascade: from receptor-mediated mitotic signals and transphosphorylation reactions to gene transcription and protein synthesis.[82]

Coherently with the promoting role of Mg^{2+} on protein and DNA synthesis, proliferating cells contain more Mg^{2+} than resting ones.[83]

Cell proliferation, as well as cell cycle and differentiation, require appropriate Mg^{2+} level to occur, hence they could be really compromised in non-physiological conditions influencing Mg^{2+} concentration and homeostasis. For example, Mg^{2+} deprivation induces inhibition of DNA and protein synthesis, thus leading to growth arrest. This effect is mainly due to the decreased amount of Mg^{2+} bounded to ATP. However, different cellular types vary in their dependence on the extracellular Mg^{2+} availability. In general, diploid cells are highly sensitive to changes in magnesium availability: endothelial cells and fibroblasts decreased their growth rate to a considerable extent when the cells were maintained in 0.1 mM extracellular Mg^{2+}. Intriguingly, immortalized cells, showed a 50% growth inhibition only upon exposure to 0.05 mM Mg^{2+}.[84]

Tumour cells proved to be the most resistant ones, showing an unaltered growth rate at 0.05 mM extracellular Mg^{2+}.[85]

Furthermore, it has been shown that Mg^{2+} deprivation induces an arrest of cell cycle progression in G0/G1 phase and a decreased percentage of cells in the S phase; however cell cycle arrest is reversible by adding Mg^{2+} in the culture medium. On the contrary increasing the amount of extracellular Mg^{2+} induces activation of cell cycle. It has been reported that MAP kinases protein trigger this reactivation, leading to up-regulation of cyclins D and E and decreased expression of p21 and p27.[86] The modulation of cell cycle regulatory proteins such as p21 and p27, cyclins and CDKs is a common feature of the Mg^{2+}-dependent control of cell proliferation.[87] This suggests that Mg^{2+} availability affects cell cycle by influencing the transcription of the related gene, as shown in figure 3.

To discern the complex but coordinated growth response that drives cell proliferation Harry Rubin postulated the theory of "*Membrane Magnesium Mitosis*", suggesting a role of second messenger for cytoplasmic free Mg^{2+}. The basic concept of this theory is that membrane perturbations induced by growth factors causes a decrease of Mg^{2+} binding affinity with consequent increase in intracellular Mg^{2+} levels. The release of Mg^{2+} triggers in turns protein and DNA synthesis increasing number of $MgATP^{2-}$ dependent reactions, ultimately leading to cell division. In this view, Mg^{2+} acts as a direct regulator of cell proliferation.[88]

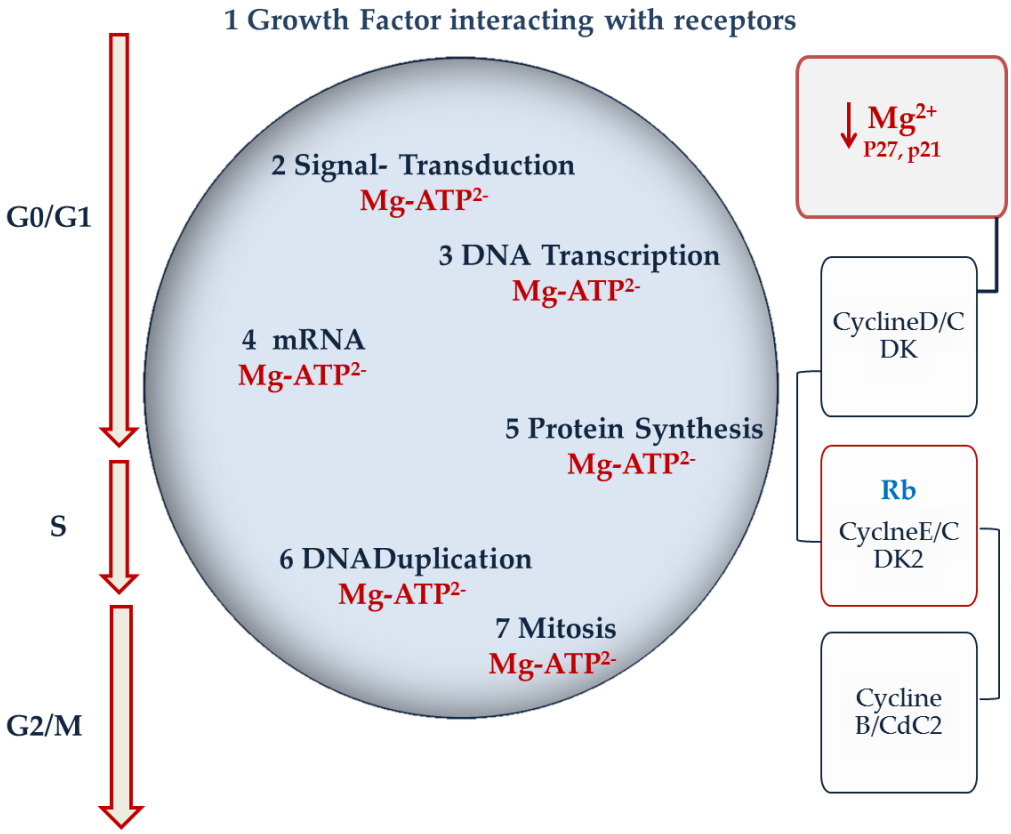

Figure 3 Pathway of cell proliferation and its regulation by Mg^{2+}. Mg availability may affect all steps leading to cell proliferation, from signal transduction to mitosis. At the molecular level, low Mg up-regulates p27 and p21 inhibitory proteins, leading to cell cycle arrest through inhibition of cyclin/CDK complexes and consequent inhibition of the Rb (retinoblastoma)-regulated restriction point. (Adapted from Wolf et al.2008)[87]

1.4.3 Magnesium and Apoptosis

Increasing evidences indicate a potential role for Mg^{2+} cation in the apoptotic process; however, the available literature is limited and often ambiguous.

Both intrinsic and extrinsic pathways of apoptosis have been shown to be accompanied by variations in cytosolic magnesium, most of all in the early stages of the process.[87] We recently reported a decrease of both free and total magnesium during mitochondria-mediated apoptosis in colon cancer cells concomitant with increased level of Reactive Oxygen Species (ROS).[89,90] In this conditions, the analysis of the early events characterizing the trigger of apoptosis showed that, while the decrease in the total content were maintained, free Mg^{2+} levels correlated with $\Delta\Psi_m$ variations.[91]

These data are in agreement with that described by *Li et al.* reporting that a decline in free cytosolic Mg^{2+} was observed during peroxynitrite-induced apoptosis in rat aortic smooth muscle cells.[92] Furthermore, it has been shown that Mg^{2+} deprivation in rat hepatocytes induces apoptosis by an increased susceptibility to oxidative stress provoked by a decrease in glutathione concentration and an increase in lipid peroxidation.[93] On the other hand, several studies have indicated a promoting role for Mg^{2+} in apoptosis; it was hypothesized that apoptosis is promoted by an influx of Mg^{2+} which stimulates the activity of nuclear endonucleases.[94] Moreover, Mg ions seems to potentiate the release of proapototic factors from the mitochondria.[95]

Given the pivotal role of mitochondria in the apoptotic process, the presence of a selective Mg^{2+} channel in the inner mitochondrial membrane, MRS2, which activity is regulated by $\Delta\Psi_m$ status, strongly suffrages the hypothesis of Mg^{2+} involvement in the apoptotic onset.

Other evidences point to an involvement of Mg^{2+} in the prevention of apoptosis. It has been showed that the administration of magnesium sulphate inhibits

caspase-3 activation and exert antiapoptotic effect after hypoxia-ischemic brain injury in rats and reduced neuronal apoptosis. [96,97] Accordingly, it has also been demonstrated that magnesium sulphate administration attenuates the marked alteration of the ratio of Bax and Bcl-2 protein during hypoxia. [98] This data suggests that magnesium sulphate treatment before and during hypoxia may decrease programmed cell death by keeping constant Bax / Bcl-2 ratio.

1.4.4 Magnesium and Cancer

Tumour tissues are characterized by high proliferation rate, dedifferentiation and invasiveness.[99] All these process need energy to occur and consequently Mg^{2+} availability.

In particular, Mg^{2+} involvement in carcinogenesis is mainly due to Mg^{2+} deficiency conditions responsible for increasing of inflammation and free radicals levels leading to oxidative DNA modifications and mutagenesis. Moreover, Mg^{2+} deficiency can be also responsible of defects in DNA repair mechanisms which dysfunction compromises genomic stability leading to genomic alterations.[74] On the other hand, magnesium could exert also protective effect in the early stage of carcinogenesis as magnesium hydroxide supplementation reduces the incidence of colon cancer in animal models.[100]

Once the process of carcinogenesis is concluded, all the efforts are directed to inhibit tumour growth and angiogenesis. Many findings are consistent to a protective role of low magnesium availability. Unfortunately, the beneficial effects of low magnesium in tumour cell proliferation and neo-angiogenesis are counterbalanced by the higher possibility to develop metastasis.[101]

Referring to normal cells, they show a correlation of the growth rate with magnesium availability; in contrast, tumour cells are completely independent from this parameter and ceased to proliferate only when extracellular

magnesium is very low. Unbalanced magnesium homeostasis is frequently observed in tumour cells that accumulate Mg^{2+} at the expenses of plasma or normal tissues. Tumour cells show great affinity for Mg^{2+} even when cultured in low magnesium concentration. The propensity of neoplastic cells to accumulate Mg^{2+} may be due to the wrong function of cellular extrusion mechanisms or to the overexpression of influx channels.[102] The most accredited influx channel involved in cancer is TRPM7.[52]

TRPM7 seems to be required for proliferation of several types of tumour cells, including leukaemia, retinoblastoma, and carcinoma cells of pancreatic, breast, gastric and head and neck origins. Furthermore increased TRPM7 expression was found in human breast and pancreatic adenocarcinoma tissues, where it correlated with clinic pathological parameters, such as tumour grade and patient survival.[103]

Interestingly, it has been suggested that hypomagnesemia could be considered a predictive factor of efficacy and outcome in colorectal cancer patients treated with cetuximab+irinotecan. In fact, those patients with an early decrease of serum Mg^{2+} ion presented better median time to progression and longer overall survival (OS) to patients with <20% reduction of serum magnesium.[104] In the light of requirement of magnesium in tumour growth, these findings suggest that magnesium deficiency could be used parameter for the efficacy of the treatment avoiding a costly a potentially toxic administration in non-responder patients.

1.4.5 Magnesium and Drug Resistance

Multi drug resistance is a phenomenon characterized by the ability of drug resistant tumours to exhibit simultaneous resistance to a number of structurally and functionally unrelated chemotherapeutic agents.[105] MDR is the principal

mechanism by which many cancers develop resistance to chemotherapy drugs and the major factor in the failure of many forms of chemotherapy. Resistance to therapy has been correlated to the presence of at least two molecular "pumps" in tumour-cell membranes that actively expel chemotherapy drugs from the intracellular compartment. This allows tumour cells to avoid the toxic effects of the drug on molecular processes within the nucleus or the cytoplasm.[106]

While the original role for these proteins was to protect animals from xenobiotics, MDR pumps might also transport "normal" substances, such as steroids and some fats, out of cells. The two pumps commonly found to confer chemoresistance in cancer are P-glycoprotein (P-gp) and the so-called multidrug resistance–associated protein (MRP). High expression of P-gp has been observed in LoVo colon cancer cells resistant to doxorubicin. Furthermore, P-gp was found in the plasma membrane, in the intracellular membranes, and in the nuclear envelope of LoVo resistant cells.[107] However, it has becoming increasingly evident that there are probably other multidrug resistance–inducing macromolecules in cancer cells that have not yet been characterized.[108]

Most cytotoxic chemotherapeutics eliminate tumour cells by activating the intrinsic apoptotic pathway.[109] In this view, success of many therapeutic agent depends on the ability to induce apoptosis as one of the proposed mechanism by which cancer cells develop resistance to drugs is the defect of apoptosis signalling.[110] Tumour cells can acquire resistance to apoptosis by the expression of anti-apoptotic protein such as Bcl-2 or by down-regulation or mutation of pro-apoptotic protein such as Bax.

Wide ranges of mechanisms have been suggested in overcoming drug induced apoptosis. In this regard Mg^{2+} may play a role.

In particular, it has been proposed a role for the mitochondrial Mg^{2+} channel MRS2 in circumventing drug induced apoptosis in gastric cancer cells. [45]

It has been shown that MDR gastric cancer cells present an up-regulation of the gene codifying for MRS2 protein compared to its parental cells.[47] Furthermore, MRS2 transfection was shown to confer an MDR phenotype to gastric cancer cells; vice versa, MRS2 knock down partially reversed the MDR phenotype in cells with acquired resistance. In view of these findings, the most accepted hypothesis is that overexpression might counteract drug-induced apoptosis by increasing magnesium influx into mitochondria.[111]

Notably, increased magnesium content has been reported in tumour mitochondria or cells. It has also been shown, that a cis-platin resistant human ovarian carcinoma cell line (C13*) presents a significantly higher Mg^{2+} content than the sensitive parental cells. Since mitochondria, along with nuclei and microsomes, represent preferred compartments of Mg^{2+} accumulation, mitochondria alterations acquired by C13* cells during resistance selection may at least partly account for their elevated Mg^{2+} concentration compared to sensitive cells.[112] An alternative, but not mutually exclusive, hypothesis is that magnesium could potentiate mitochondrial energetic function and consequently the activity of efflux pumps, which are highly dependent on ATP.[103]

1.5 Intracellular magnesium determination

Although magnesium is essential for a number of biological processes crucial for cell life, its distribution and intracellular compartmentalization have not been elucidated yet, mainly because of the lack of suitable analytical methods. Furthermore, Mg^{2+} seems to be well buffered within the cytoplasm implying that Mg^{2+} fluctuations could only be traced by techniques able to sense minor changes.[113]

To date, the most common approach to assess total cellular magnesium in the cell or tissue is by Flame Atomic Absorption Spectroscopy (F-AAS) on acidic extracts, a technique that requires large samples (at least millions of cells or several milligrams of tissue). Other more sensitive techniques require smaller sample sizes, such as Inductively Coupled Plasma Mass Spectroscopy (ICP-MS) and Graphite Furnace AAS (GF-AAS). These techniques indubitably offer improved detection limits, however require instrumentations not easily available in any laboratory, complex analytical procedures and specific technical skills and competencies.[114]

Another method to assess the intracellular concentration of Mg^{2+} is by phosphorus magnetic resonance spectroscopy31P NMR. This technique is based on the fact that most of magnesium in the cytosolic matrix is bound to ATP. Therefore variation in the acquired chemical shift associated to the phosphorylated molecule present in the cytoplasm including Inorganic Phosphate (Pi), Phosphocreatine (PCr) and ATP depends on the Mg^{2+} concentration. While non-invasive, 31P NMR measures Mg^{2+} indirectly averaging over a large collection of cells.[115]

1.5.1 Fluorescent chemosensors

Although the importance of Mg^{2+} is widely acknowledged, all the efforts in developing fluorescent probes have been made to study and monitor Ca^{2+} concentration *in vivo*, as fast-acting principal second messenger; therefore, Mg^{2+} has become the "forgotten" cation in human health. Hence, the development of Mg^{2+} selective probes derived from the cross reactivity of Ca^{2+} probes. [113]

Therefore, the design of highly selective Mg^{2+} fluorescence probes is an intriguing challenge as is confirmed by the last development in this field.[116]

The first developed fluorescent Mg^{2+} indicators, APTRA (*o*-amminophenol-*N*,*N*,*O*-triacetic acid) family and it derivatives, are structural analogues of Mg^{2+} chelator EDTA (ethylendiaminetetraacetic acid); these molecules have been used as ^{19}F NMR indicators. Subsequently, the APTRA structure has been modified around the furan ring resulting in the FURAPTRA (mag-fura-2) which is still used in many laboratories.[117,118] Since then, many others probes has been synthetized to be selective for Mg^{2+} ion, however they were simply analogues of the corresponding Ca^{2+} indicators.

The currently most commonly applied approach uses synthetic dyes that alter their fluorescent properties upon binding of Mg^{2+}. However, many of the available dyes show limited specificity for Mg^{2+} and often bind Ca^{2+} with low micromolar affinity, which has been shown to interfere in an intracellular setting. The AMg1 fuorescent dyes developed by *Kim et al.*, whose high two photon cross-section makes them suitable for two photon confocal microscopy, partially discriminate between membrane and cytosolic Mg^{2+}.[119]

A notable exception is the family of fluorescent molecules, *diaza-18-crown-6 8-hydroxyquinolines* derivatives (DCHQ) that show a remarkable affinity and specificity for magnesium reporting a K_d value for Mg^{2+} in the order of the micromolar range. Indeed, commercially available Mg^{2+}-specific luminescent probes are all characterized by $K_d(Mg^{2+})$ values in the millimolar range: therefore, they are suitable to detect mainly free cytosolic magnesium ions (only 5% of the total) without providing any information about total fraction. This unique characteristic of DCHQ molecules, permit to detect total intracellular magnesium giving a concentration value fully comparable to that obtained with AAS. The most promising derivative of this family is the DCHQ5 chemosensor which presents many advantages including the high intracellular retention or the possibility to avoid the UV excitation which could be potentially cytotoxic, as it could be excited both in the UV and Visible wavelength regions. [120]

Among fluorescent chemosensors, particular interest has been recently raised by KMG-104 and related dyes developed by *Kuzuki and coworkers*, whose affinity for Mg^{2+} is higher than for Ca^{2+}, rendering these dyes completely insensitive to physiological changes in cytosolic Ca^{2+} concentration. Recently a variant of this dye, KMG-103 was reported to show preferred accumulation in mitochondria.[121]

Last development in the field of fluorescence chemosensor is referred to the genetically encoded metal sensors based on the Förster Resonance Energy Transfer (FRET). These sensors do not require cell-invasive procedures, their concentration can be tightly controlled and they can be targeted to different locations in the cell. In particular, the first developed genetically encoded fluorescent sensor (MagFRET-1) for Mg^{2+} shows a 50% increase in emission ratio upon Mg^{2+} binding. A general advantage of genetically encoded sensors is that their subcellular localization can be easily controlled.

Although MagFRET-1 is responsive to changes in Mg^{2+} concentration in permeabilized cells, for some unknown reason MagFRET-1 is less responsive in intact cells. Moreover, MagFRET-1 responds to changes in Mg^{2+} concentration in the order of seconds both *in vitro* and in cells, but miss sensitivity for changing in overall Mg^{2+} levels over longer periods of time. These changes may be more reliably monitored using lifetime imaging (FLIM), which might also be the preferred method to allow quantification of intracellular Mg^{2+} concentrations.[122] Even though this technique allows to study Mg^{2+} variations in the intracellular compartment of a single cell it does not give an absolute quantification of the element.

1.5.2 X-Ray microscopy

Recently, one of the main focus of life science in elemental quantification is direct to single cell analysis. Indeed, the possibility to have a map of whole single cells could give important information about morphology of the cell, amount of element constituting the cell and more important elemental distribution and compartmentalization in the cell organelles. [123]

Knowledge of the distribution of the chemical elements in organelles may reveal their function in a variety of cellular processes. Element imaging can be achieved by use of several micro-analytical techniques, for example histochemical techniques, radioisotope imaging, magnetic resonance imaging, mass spectrometry imaging, and microprobe X-ray fluorescence imaging.

Apart from the aforesaid MagFRET-1, magnesium content in different subcellular compartments can be evaluated by electron probe microanalysis (EMPA) which operates by using an electron microscope and bombarding a micro-volume of a sample with a focused electron beam (typical energy = 5-30 keV) and collecting the X-ray photons thereby emitted by the various elemental species. Because the wavelengths of these X-rays are characteristic of the emitting species, the sample composition can be easily identified by recording WDS spectra (Wavelength Dispersive Spectroscopy).[124]

Another technique proved its usefulness for element imaging and speciation analysis in eukaryotic cells is the X-ray microspectrometry methods based on synchrotron radiation [125]

Micro and nano-SXRF (synchrotron X-ray fluorescence) can be used for imaging element distribution at high spatial resolution (<100 nm), and micro-XAS (X-ray absorption spectroscopy) has quite unique capability for direct determination of element speciation in cellular compartments, because it can be used to probe the local structure of the absorbing element with high chemical sensitivity. The increased spatial resolution of these methods achieved in recent years now

enables imaging of element distribution within the main cellular organelles, nucleus, Golgi apparatus, endoplasmic reticulum, vacuoles, lysosomes, mitochondria, and chloroplasts. However, identification by optical microscopy before X-ray imaging is usually limited to the larger organelles, i.e. the nucleus, the cytoplasm, and the vacuole. By using the principles of this technique a new developed method allows to address Magnesium in subcellular compartments. This new method combines X-Ray fluorescence microscopy and Scanning transmission X-Ray Microscopy to Atomic Force Microscopy and has been made thanks to the availability of synchrotron radiation sources and improvements in X-ray optics.[126]

2 APOPTOSIS

2.1 Introduction

The term “apoptosis” is derived from the Greek words “απο“ and “πτωσιζ“ meaning “dropping off” and refers to the falling of leaves from trees in autumn. It is used, in contrast to necrosis, to describe the situation in which a cell actively pursues a course toward death upon receiving certain stimuli.[127,128]

Kerr et al firstly described apoptosis as an active and highly organized form of cell death characterized by biochemical events of removing stressed or damaged cells within multicellular organisms that result in specific morphological changes.[129,130]

This form of cell death is characterized by membrane blebbing, cell shrinkage, nuclear fragmentation, chromatin condensation and chromosomal DNA fragmentation. This process, which plays a crucial role in embryonic development, is necessary to maintain tissue homeostasis as its deregulation results in a variety of diseases including tumorigenesis. [131]

Moreover, evasion of apoptosis is one of the hallmarks of cancer and confers drug resistance to cancer cells. Apoptotic mechanisms are divided into two main pathways.[132] The ‘‘extrinsic pathway’’ is activated by extracellular death ligands and cognate death receptors (e.g., tumor necrosis factor-a [TNF-a]); and the ‘‘intrinsic pathway,’’ which responds to intracellular stress signaling (e.g., macromolecular damage), is mediated by mitochondria.

During the intrinsic pathway of apoptosis, the permeabilization of the mitochondrial membrane and the consequently release of pro-apoptotic factors ultimately lead to the activation of a special class of cleaving enzyme called caspase, representing a point of no return in apoptosis. Caspases are a family of

cysteine proteases with roles in apoptosis, inflammation, and development. In healthy cells, caspases reside in the cytosol as inactive pro-enzymes and direct association with molecules of the inhibitor of apoptosis protein (IAP) family maintains their inactive state.

This class of enzyme, are involved both in the intrinsic and in the extrinsic pathway of apoptosis. Caspase-8 and caspase-9 are the initiator caspases of the extrinsic and intrinsic apoptosis pathways, respectively, that in turn mediate activation of the executioner caspase-3 to evoke many of the defining biochemical and biophysical changes that occur during apoptosis.

2.1.1 Intrinsic Pathway of Apoptosis

The intrinsic apoptotic pathway can be activated by range of stress stimuli, including UV radiation, ROS, DNA-damaging agents or activation of oncogenic factors.[132] The key event of this process, which is also known as mitochondria mediated apoptosis, is the mitochondria outer membrane permeabilization (MOMP).

When in 1990, the anti-apoptotic function of the oncogene B cell lymphoma 2 (Bcl-2) were found to be implicated in the commitment of this membrane permeabilization, regulation of apoptosis at mitochondria level emerged as a great opportunity for intervention in pathological conditions such as cancer.

In particular, Bcl-2 proteins control MOMP by acting as either inhibitors or activator of the apoptotic process. [133]

At molecular level, two pro-death members of the Bcl-2 family, Bax and Bak induce the MOMP. These proteins oligomerize and are inserted into the outer membrane of mitochondria, which disrupt organelle membrane potential and also induce a rapid release of cytochrome *c*, Smac/DIABLO, and HTRA2/O from the intermembrane space into the cytosol.

Through MOMP, the pro-apoptotic inter membrane space proteins relocalize to the cytosol to initiate caspase activation, and this process generates the mitochondrial signal required for the intrinsic pathway to proceed.
In particular, cytochrome c forms a complex with APAF-1 and pro-caspase 9 named "*apoptosome*", whereas Smac/DIABLO binds to inhibitors of apoptosis proteins (IAPs). Consecutively, the executioner caspase-3 is recruited to the apoptosome, where it is activated by the resident caspase-9. Caspase-3 then cleaves key substrates in the cell to produce many of the cellular and biochemical events of apoptosis.[134]

2.1.2 Extrinsic Pathway of Apoptosis

The extrinsic pathway of apoptosis is mediated by ligands activating death receptors (DR). Death receptors belong to the tumour necrosis factor (TNF) receptor superfamily, and include functional receptors and decoy receptors. The receptor superfamily includes TNF-R1, Fas/APO1, DR3, TNF-related apoptosis-inducing ligand receptors-1 (TRAIL-R1, DR4), -2(TRAIL-R2, DR5), and DR6. Others TNF receptors regulate several biological functions including cell metabolism, proliferation and cytokine production. These death receptors have an intracellular death domain that recruits adapter proteins such as TNF receptor-associated death domain (TRADD) and Fas-associated death domain (FADD), as well as cysteine proteases like caspase 8. Ligation and oligomerization of Fas, TNF receptor 1, or the TRAIL receptor triggers formation of a receptor-associated death-inducing complex (DISC) for recruitment and activation of caspase-8 and 10. High levels of active caspase-8 generated by large amounts of procaspase-8 processing at the DISC lead to the activation of executioner caspases, including caspase-3, and the induction of apoptosis. Activation of caspase-8 can also result in the cleavage of the BH3-

only protein BID to generate the activated BID fragment tBID, which serves to transmit the death signal from the extrinsic to the intrinsic signaling pathway.(see Fig. 4).

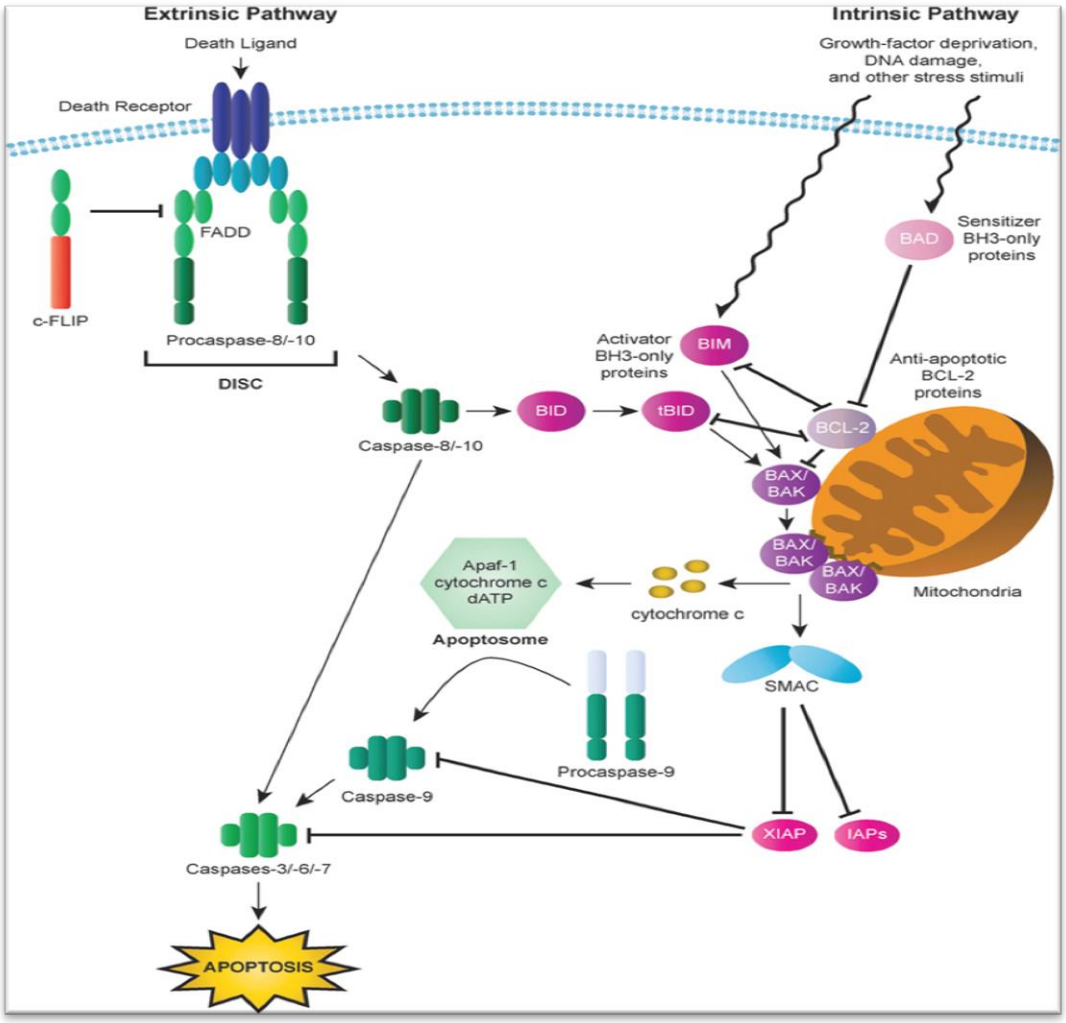

Figure 4 Intrinsic and Extrinsic pathway of apoptosis[132]. In the intrinsic pathway, mitochondrial outer membrane permeabilization (MOMP) results in the release of cytochrome c and other apoptogenic factors from mitochondria into the cytosol and the ensuing formation of the apoptosome, which triggers activation of the apoptosis-inducing caspase cascade via activation of caspase-9. In the extrinsic pathway, binding of death receptors such as FAS or TRAIL receptors by their cognate ligands triggers the recruitment of death domain (DD)-containing adaptor proteins (represented by FADD) and procaspases with a death effector domain (DED), specifically procaspase-8 and procaspase-10. The resulting complex is known as the death inducing signaling complex (DISC). High levels of active caspase-8 generated by large amounts of procaspase-8 processing at the DISC lead to the activation of executioner caspases, and the induction of apoptosis.

2.2 Apotosis in cancer therapy

Cancer is the result of a succession of genetic changes during which a normal cell is transformed into a malignant one; the hampering of cell death is one of the essential changes that cause this malignant alteration. Hence, reduced apoptosis or its resistance is an important link of the triggering of carcinogenesis.

Defects in the apoptotic process is also a very common cause of resistance to anticancer drugs. Therefore, apoptosis is a fundamental parameter to be considered in the treatment of cancer and represents a popular target of many treatment strategies.

There are many ways a malignant cell can acquire reduction in apoptosis or apoptosis resistance such as disrupted balance of pro-apoptotic and anti-apoptotic proteins, reduced caspases function and impaired death receptor signalling. Many proteins have been reported to exert pro- or antiapoptotic activity in the cell. Imbalance or dysregulation of these proteins have been found to contribute to carcinogenesis by reducing apoptosis in cancer cells. [127]

Disruption in the balance of anti-apoptotic and pro-apoptotic members of the Bcl-2 family, results in deregulation of apoptosis. Moreover, it has been suggested that the loss of caspases-3 expression and function could contribute to breast cancer cell survival. [135]

Among intracellular organelles, mitochondria play a pivotal role in apoptosis, as a consequence damage to these organelles or to mitochondrial DNA may promote tumors formation by the inhibition of apoptosis of pre-cancerous cells. Indeed it has been found that cells lacking of mitochondrial genome, defined as *rho0* cells, are less sensitive toward different apoptosis-inducers, including staurosporine, doxorubicin, daunomycin and quercetin, when compared to parental cells. [136]Furthermore, rho0 cells exhibit over-expression of multidrug

resistance 1 (MDR1) gene and its product P-glycoprotein (P-gp). Combined with standard anticancer strategies, application of compounds directly affecting mitochondrial functions is a promising approach for eradication of chemotherapy-resistant cancer cells.

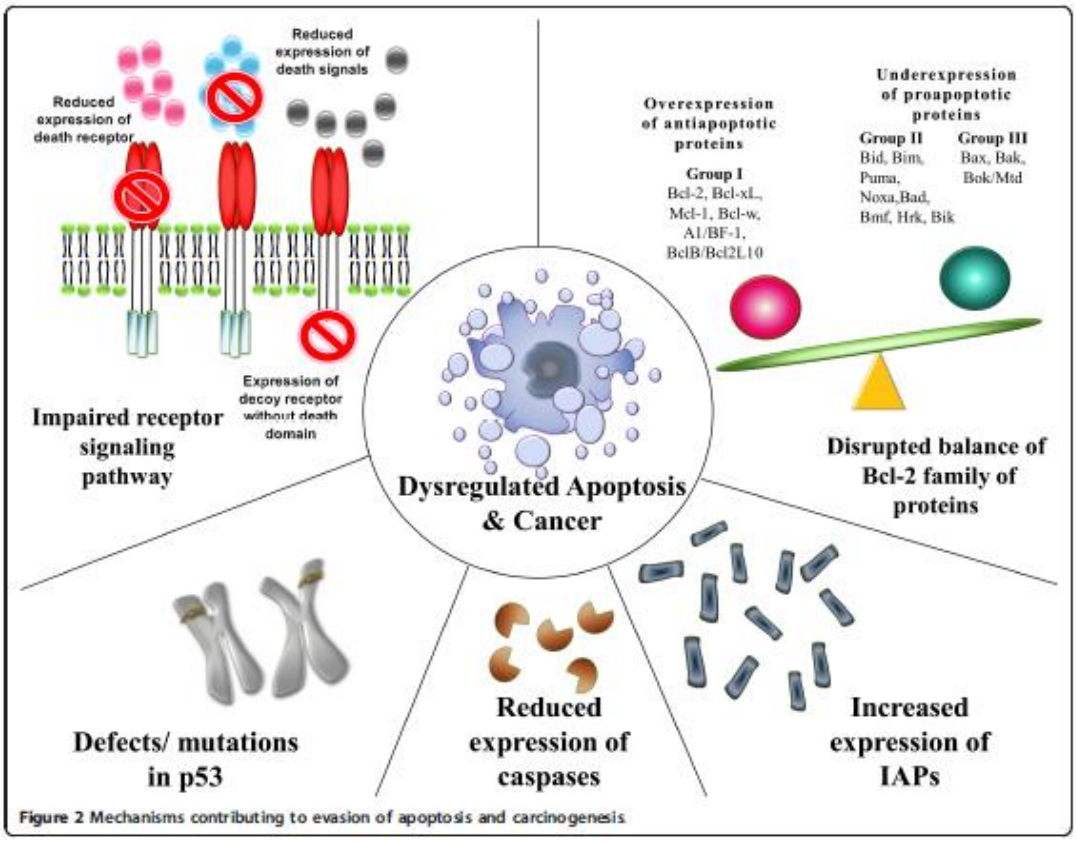

FIGURE 5 **Mechanisms of evasion from apoptosis**

3 AIMS

Understanding apoptosis mechanisms may give insights into the pathogenesis of many disease and may leave indications on how the disease can be treated.[127]

In the case of tumour treatment, most of the cytotoxic chemotherapeutic agent eliminates tumour cell by activating the mitochondrial apoptotic pathway.[137] However, prior to this terminal stage of apoptosis cells fight to resist pharmacological insults.

In certain conditions, cancer cells develop the possibility to avoid apoptosis induction and become resistant to the administrated drug and to other unrelated drugs. This phenomenon is termed *multi drug resistance* (MDR). The acquired or intrinsic MDR is the major obstacle in achieving the effective chemotherapy in malignant tumours. However, the mechanisms of MDR remains obscure.[45]

Because of the pivotal role of mitochondria in apoptosis, they are also involved in tumour formation by the inhibition of apoptosis of pre-cancerous cells.

Indeed, mutations in genes involved in the regulation of the mitochondrial pathway are very common in cancer cells and mitochondrial ion channels are emerging as promising targets for cancer treatment.[138] Among mitochondrial ion channels MRS2 is the only known Magnesium transporter in mitochondria. Interestingly, the expression of MRS2 channel has been associated with resistance to drug-induced apoptosis in cancer cells.[139]

It is worth remembering that mitochondria are the major Mg^{2+} store in the cell.[15]

Considering the prominent role of Mg^{2+} in cell proliferation it is evident that perturbations in the intracellular Mg^{2+} concentration could have serious implications for the proper functioning of cells.

Thus, the involvement of Mg^{2+} cation changes could result in altered Mg^{2+} compartmentalization and mobilization and might eventually modify the progression of apoptosis.

In the first part of the project, carried out in collaboration with Dr. Martin Kolisek and Dr. Gerhard Sponder, at the Free University of Berlin, we investigated the involvement of magnesium and its mitochondria transporter MRS2 in the apoptotic process, eventually leading to multi drug resistance phenotype.

Aimed to reach a regulated expression of MRS2 we generated an appropriate transgenic cellular system by using human embryonic kidney cells (HEK-293). After checking the induced protein expression we performed Mg^{2+} uptake experiments in isolated mitochondria to confirm the influx activity of the channel. Furthermore, aimed to verify if modulation of this channel could have an impact also on the total amount of cellular Mg^{2+}, we examined total intracellular Mg^{2+} content in cells overexpressing MRS2.

However, the main goal of this research was to investigate whether MRS2 could influence the sensitivity to apoptotic treatment. Cells transiently overexpressing MRS2 were exposed to two commonly used molecules in chemotherapy able to induce apoptosis; the efficacy of the drugs and the eventually anti apoptotic effect of Mg^{2+} channel were evaluated by cell cycle analysis, morphological analysis and caspase activity assay.

The second part of this research was aimed to verify whether magnesium intracellular content and compartmentalization could be used as a signature to distinguish MDR tumour cells from their drug-sensitive counterparts.

To accomplish this objective we have chosen a tumour cell line, more appropriate for studies on the MDR phenotype.

Measurements on LoVo human colon cancer cells sensitive (LoVo-S) and resistant (LoVo-R) to doxorubicin were performed to investigate cellular Mg^{2+} concentration changes in MDR tumour cells to better understand the involvement of Mg^{2+} in multi-drug resistance.

We exploited a standard-less approach providing a complete characterization of whole single-cells by combining X-Ray Fluorescence Microscopy (XRFM), Atomic Force Microscopy (AFM) and Scanning Transmission X-ray Microscopy (STXM). This method allows the quantification of the intracellular spatial distribution and total concentration of magnesium in whole dehydrated cells. Subsequently, aimed to compare single cells analysis with large cell population we quantified the total amount of intracellular Mg^{2+} in a large populations of cells by using DCHQ5 probe and traditional fluorimetric technique.

4 MATERIALS AND METHODS

Part I

4.1 Cell Culture and reagents

Clone 2 cells derived from Human Embryonic Kidney cells (HEK-293) were grown in Dulbecco's modified Eagle's medium (DMEM) containing 4.5 g/l glucose, 3.7 g/l NaHCO3 and 110 mg/l pyruvate, supplemented with 10% fetal bovine serum (FBS, Biochrom) L-glutamin 2mM, penicillin 100 U/mL and streptomycin 100 μg/mL. Cultures were kept at 37°C in 5% CO2 atmosphere. Recombinant human MRS2 was purchased Synthesisgene. Doxorubicin hydrochloride was purchased from Sigma Aldrich and dissolved in sterile ultrapure water and stored at -20°C.

Staurosporine was purchased from Sigma Aldrich as film, dissolved in Methanol and stored at 4°C. The concentration of the solutions was assessed by spectrophotometer assays.

4.2 T-REx™ System

HEK-293 cells were stably transfected with pcDNA6™/TR (Invitrogen) plasmid and selected with blasticidin (Labogen).[140] Before transfection, the sensitivity of HEK-293 cells to blasticidin was evaluated.

The pcDNA6™/TR vector expresses high levels of the Tet repressor gene which enables the host cell line to keep the protein expression levels very low before

the tetracycline induction; the plasmid includes as well the blasticidin resistance gene under the control of the SV40 promoter which allows the selection of cells stably transfected with the plasmid. The pcDNA6™/TR was transfected into HEK-293 cells using Polyethylenimine (PEI) as transfection reagent and the cells, which had stably integrated the vector in their genome and which therefore express the Tet repressor, were selected using blasticidin 15 µg/mL.
The generated cell line stable transfected with pcDNA6™/TR vector were named "Clone 2".

4.3 Cell growth curves

HEK-293 cells and their stable transfected counterpart Clone 2, were trypsinized, centrifuged and the pellet was resupsended in 2.5 mL of medium. The cells were counted by using Hemocytometer every 24 hours.
The population-doubling time has been determined by identifying a cell number along the exponential phase of the curve, tracing the curve until that number has doubled, and calculating it by the following equations:

$$n = \frac{logNt - logN0}{log2}$$

Eq.1

$$DT = \frac{T}{n}$$

where *Nt* cell number at certain time point *t*

N0 cell number at time point 0

T is the exponential time phase

n number of generation

4.4 Cell transfection

The blasticidin selected cells, "Clone 2", has been used as Tet repressor expressing cell line for the following experiments requiring a well-regulated over-expression of *MRS2*. Clone 2 cells were grown in the above-mentioned DMEM supplemented with 15 μg/mL blasticidin in order to keep the Tet repressor selection.

Transiently over-expression of MRS2 was performed in Clone 2 by transfection with the pcDNA5™/TO-MRS2 vector under the control of cytomegalovirus (CMV) promoter and tetracycline operator sites.[141] Protein expression was induced by addition of tetracycline (Sigma, Sigma-Aldrich, St Louis, MO, USA) to a final concentration of 1 μg/ml.

4.4.1 Plasmid Constructs

The MRS2 gene was synthesized and cloned via a 5′ KpnI and a 3′ XhoI restriction site into pcDNA5™/TO. For transfections, all the recombinant plasmids were prepared using the NucleoSpin Plasmid Kit (Macherey-Nagel) and polyethylenimine (Sigma-Aldrich) was used as transfection reagent the appropriate ratio of plasmid DNA to PEI was calculated with the online calculation tool: http://www.cytographica.com/lab/PEItransfect.html. Plasmid DNA was transfected to HEK-293 cells grown in a 25 cm2 flask and the cells were incubated for 24 hours before induction of protein expression.

4.5 Western Blotting analysis

Clone 2 cells were detached and centrifuged at 1200 RPM for 5 min, the pellet was resuspended in 20μL of RIPA buffer plus protease inhibitor. After 7 min on ice, cells were resuspended by vortexing, then incubated on ice for 7 min

and resuspended again. Soluble proteins were separated by centrifugation at 14000 g for 20 min at 4°C. The protein concentration was quantified by the 660 nm Protein Assay Kit (PIERCE, Rockforfd, IL).

The extracts were resuspended in 2X SDS sample buffer were and separated on a 8.5% sodium dodecyl sulfatepolyacrylamide gel electrophoresis (SDS-PAGE). The Page Ruler Prestained Protein Ladder 10 to 170 kDa (Thermo Scientific) was also loaded on the gel as a molecular weight standard.

Proteins were then transferred to a polyvinylidene fluoride (PVDF) membrane by standard procedure. RPL expression (Ribosomal Protein) has also been evaluated as loading control.

Membranes were blocked with 5% non-fat milk in TBS-T (10 mM TrisHCl, pH 8.0, containing 150mM NaCl + 0.1% Tween 20) solution for 2 hours at room temperature (25°C). After washing with TBS-T , the membranes were incubated with a primary antibody directed against the Strep- tag at 4°C on a shaker. After overnight incubation the membranes were washed with TBS-T, immunoblots were then incubated with a secondary HRP-conjugated anti-mouse antibody 1:1000 (Cell Signaling technology, Danvers, MA, USA) and Strep-tagged proteins were visualized by using SuperSignal West Dura Extended Duration Substrate (Pierce Biotechnology, Rockford, IL, USA) according to the manufacturer's instructions.

4.6 Mitochondria isolation

Cells were harvested by centrifugation (300gav, 4 min at 4°C) and resuspended in cold isolation buffer (IB) (210 mM mannitol, 70 mM sucrose, 5 mM Hepes-KOH pH 7.2) with 0.25% BSA (fraction V). The cells were centrifuged again (300gav, 4 min at 4°C) and resuspended in IB (4mL/gram cells). Cells were permeabilized by addition of 20µl digitonin (1 mg/ml). After reaching the

permeabilization of 0.2-0.4 mg/mL by subsequent addition of 20µL digitonin, 5mL of IB were added. The cell suspension was washed and then broken in a Dounce-homogeniser in ice. The pellet was resuspended in IB w/o BSA and cell debris were removed by repeated low speed centrifugation (1200 g for 3 min.). Mitochondria were collected by centrifugation of the remaining supernatant (3500gav for 20 min., 4°C) to obtain the heavy mitochondrial fraction and 10.000gav, 10 min, 4°C, to obtain the light mitochondrial fraction.[142]

The pellet containing mitochondria was resuspended in 1 mL of IB supplemented with ATP 0.5 mM, Succinate 0.2% and Pyruvate 0.01%.

4.7 Spectrofluorimetric Analysis

For the fluorescence spectroscopy measurement, uncorrected emission and corrected excitation spectra were obtained with a PTI Quanta Master C60/2000 spectrofluorimeter (Photon Technology International, Inc., NJ, USA) and with PerkinElmer spectrofluorimeter.

4.7.1 Measurement of mitochondrial magnesium uptake

Loading of mitochondria with mag-fura 2-AM

Loading was performed by incubating 1 mL of mitochondria suspension with 5 µM of mag-fura 2-AM plus 1 µL of Pluronic (Eugene, OR) for 25 min at room temperature. After the incubation period, mitochondria were washed twice in IB w/o BSA to remove excess dye and resuspended in the same buffer supplemented with ATP 0.5 mM, Succinate 0.2% and Pyruvate 0.01%. Afterwards, the mitochondria were incubated for further 35 minutes to allow the complete hydrolysis of the dye, and washed twice prior to the measurement. . Measurements were performed in 3 ml cuvettes with 2 ml cell suspension at 37°C in a spectrofluorimeter LS50-B (Perkin Elmer). Data

analysis was carried out by using the FL Win Lab version 3.0 (Perkin Elmer) according to *Kolisek et al.*.[42]

4.7.2 Quantification of total cell magnesium and cell volume determination

Total magnesium content was assessed on sonicated cell samples by using the fluorescent chemosensor DCHQ5 assay as reported by *Sargenti et al*. [113] Briefly, DCHQ5 was dissolved to a final concentration of 15 μM in a mixture which contains 10% of DPBS in a solution 1:1 of MeOH:MOPS 2 mM (pH 7.4). Different amounts of $MgSO_4$ were added and the fluorescence intensities were acquired at 510 nm. The total Mg^{2+} concentrations of the unknown samples were obtained by the interpolation of their fluorescence with the standard curve.

To evaluate the mean cellular volume, Clone 2 cells were counted on a double-threshold Z1 Coulter Counter (Beckman Coulter, USA) and the thresholds were set to cover the interval from 65 to 3,600 fl, each step corresponding to an increase of 2 μm in cell diameter. The mean cellular volume was estimated from the Gaussian distribution of the data.

4.8 Microscopy Staining

4.8.1 MRS2 overexpression

Clone 2 cells were washed three times with PBS and then fixed using 2.5% paraformaldehyde in PBS for 20′ at room temperature. After washing with PBS, the cells were blocked in blocking buffer containing 10% (v/v) normal goat serum (NGS) in PBS. To determine the localization of MRS2, the cells were incubated for 1h at room temperature with the monoclonal Strep-tag primary antibody (1:500) (Qiagen). Bound anti-Strep was visualized with AlexaFluor-

488- labeled goat anti mouse (1:500) (Invitrogen). The cells were sealed using mounting medium containing 4',6 diamidino-2-phenylindole (DAPI), which stains nuclei and visualized with a fluorescence microscope.

4.8.2 Apoptosis assay on fixed cells

After 24 hours of induction with tetracycline, Clone2 cells were incubated with Staurosporine 2μM and Doxorubicin 2.5 μM for 6 and 17 hours respectively at 37°C. The coverslips were washed 3 times in phosphate-buffered saline (PBS), fixed with 4% paraformaldehyde (Sigma, USA) in PBS and permeabilized with 0.5% Triton X-100 (Sigma, USA) in PBS for 5 min at 4 °C. After 2 washes in PBS, sample were incubated in presence of Hoechst 33432 (Sigma USA) 1 μg/mL, washed and analyzed by fluorescence microscopy.(Zeiss Axioplan).

4.9 Cell cycle analysis

Clone 2 cells were detached with 0.11% trypsin (Sigma-Aldrich, St Louis MO), 0.02% EDTA, washed twice in PBS and centrifuged. The pellet was suspended in 0.01% nonidet P-40 (Sigma, USA) 10 mg/mL RNase, and 0.1% sodium citrate (Sigma USA) and 50μ g/mL propidium iodide (PI) (Sigma, USA), for 30 min at room temperature in the dark. Propidium iodide fluorescence was analyzed using a Bryte HS flow cytometer (Biorad,UK) equipped with Hg lamp and analyzed with ModFit (Verity Software House, USA) software.

4.10 Caspase Activity assay

The activity of Caspase protease enzymes was measured by the cleavage of the fluorogenic peptide substrate AcDEVD-AMC that represents a substrate for caspase 3 and other members of the caspase family. At the indicated time points

(6 hours for STS treatment and 17 hours for DXR), cells were washed in phosphate-buffered saline, harvested in 0.1 ml of lysis buffer, and subjected to two cycles of freeze–thawing. The lysates were centrifuged for 10 min at 28,000 × g at 4 °C and the supernatant was then used to assay in duplicate enzyme activity. Extract (10 μl) was incubated for 15 min at 37 °C in a final volume of 30 μl to determine caspase activity as described in reference 143.[143]

Part II

4.11 Cell Culture and reagents

Human colon carcinoma cells LoVo, sensitive (LoVo-S) and resistant (LoVo-R) to doxorubicin were cultured in Dulbecco's modified Eagle's medium (DMEM) (Sigma), supplemented with 10% fetal bovine serum (FBS), 2 mM glutamine, 100 units/mL penicillin, and 100 μg/mL streptomycin sulfate. LoVo doxorubicin-resistant cells (LoVo-R) were cultured under the same conditions and fed once every 2 weeks with 1 μg/mL doxorubicin.

For atomic force microscopy and X-ray measurements, cells were plated at a concentration of 1×10^4 cell/cm^2 on 1 × 1 mm^2, 200-nm-thick silicon nitride (Si3N4) membrane windows, mounted on a 5 × 5 mm^2 Si frame (Silson) previously sterilized in ethanol. Cells were incubated at 37 °C in 5% CO2 for at least 24 h. Two dehydration methods were then followed. In the first case, at 50–80% confluency, cells were briefly rinsed in 150 mM KCl and then fixed in ice-cold methanol/acetone 1:1 and air-dried. In the second case, after being rinsing with 100 mM ammonium acetate, cells were cryofixed by plunge freezing in liquid ethane and then dehydrated in vacuum at low temperature overnight.

4.12 Flow cytometry

Flow cytometric measurements were performed on a Bryte HS cytometer (BioRad, UK), equipped with a Hg lamp and a filter set with an excitation band centered on 360 nm and two emission bands centered respectively on 510 nm (DCHQ5 fluorescence) and 600 nm (propidium iodide fluorescence). Cells loaded with 5 μM DCHQ5 were counterstained with 5 μg/ml propidium iodide (PI) to identify dead cells. Fluorescence was recorded using a logarithmic scale.

4.13 Quantification of total cell magnesium

Total magnesium content was assessed on sonicated cell samples by using the fluorescent chemosensor DCHQ5 as reported in *Sargenti et al.* Briefly, DCHQ5 was dissolved to a final concentration of 15 μM in a mixture which contains 10% of DPBS in a solution 1:1 of MeOH:MOPS 2 mM (pH 7.4). To obtain standard curve, different amounts of $MgSO_4$ were added and the fluorescence intensities were acquired at 510 nm. The Mg^{2+} concentrations of the unknown samples were obtained by the interpolation of their fluorescence with the standard curve, referred to the actual cell volume measured as described in the paragraph 4.16.

4.14 Cell volume determination

LoVo–S and LoVo-R detached by trypsinization, were centrifuged and resuspended in Phosphate Buffuer Saline (PBS) at the final concentration between 4000/mL and 8000/mL.

Cells volumes were calculated counting LoVo cells on a double-threshold Z1 Coulter Counter (Beckman Coulter, USA) and the thresholds were set to cover the interval from 65 to 3,600 fL, each step corresponding to an increase of 2 μm in cell diameter. The mean cellular volume was estimated from the Gaussian distribution of the data. The analysis were carried out in triplicate

4.15 Fluorescence and Scanning Transmission X-Ray Microscopy analysis

The X-Ray Fluorescence Microscopy (XRFM) and Scanning Transmission X-Ray Microscopy(STXM) measurements were carried out at the beamline Twinmic at Elettra Synchrotron (Trieste, Italy). A Fresnel zone plate focused the incoming beam (1475 eV), monochromatized by a plane grating monochromator, to a circular spot of about 600 nm in diameter. The sample was transversally scanned in the zone plate focus, in steps of 500 nm. At each step the fluorescence radiation intensity was measured by eight Si-drift detectors (active area 30 mm^2) concentrically mounted at a 20° grazing angle with respect to the specimen plane, at a detector-to-specimen distance of 28 mm. Simultaneously, the transmitted intensity T was measured by a fast-readout electron-multiplying low-noise charge-coupled device (CCD) detector through an X-ray−visible light converting system. Zone plate, sample, and detectors were in vacuum, thus avoiding any absorption and scattering by air

Acquisition Protocol Dehydrated cells mounted on the Si3N4 membrane windows were carefully examined with optical microscope and selected following these criteria: integrity, dimensions (large cells require longer acquisition time), and distance from other cells (clustered cells have been avoided because AFM measurements require some free space around the cells). AFM measurements were performed on selected cells before and after XRFM

and STXM measurements. Five STXM images were acquired on whole cells with a step size of 500 nm. In sequence XRFM, and simultaneously also STXM, were carried out with a range of 6−8 s dwell time per pixel depending on the cell size. The total acquisition time was in the range of 5−8 h (field of view of at least 20 × 20 μm; spatial resolution 500 nm). The measurement of I_0 is made on a part of the substrate free from cells, acquiring 25 points and repeating the measure five times.

Mass Fraction and Concentration Calculation

To obtain quantitative information from the measurement of fluorescence radiation, we used the fundamental parameter method.

The mass fraction $\boldsymbol{W_{Mg}}$ for each Mg^{2+} pixel p was calculated by the following expression :

Eq.2
$$\boldsymbol{W_{Mg}}(\%) = \frac{\boldsymbol{dR_i}}{\boldsymbol{\rho \cdot S \cdot dz \times Y\left(E_{0,Mg}\right) \times F_p}}$$

where $\boldsymbol{\rho}$ is the density, and $\boldsymbol{F_p}$ is the correction factor for the selfabsorption of both incident beam and fluorescence radiation.

Analogously, the concentration $\boldsymbol{M_{Mg}}$ in the single pixel p, expressed in molarity, is derived by the following expression:

Eq.3
$$\boldsymbol{M_{Mg} = w_{Mg} \cdot \frac{1}{A_{Mg}} \cdot \frac{m}{V} \cdot 10^3}$$

where $\boldsymbol{M_{Mg}}$ is the mass expressed in molarity and $\boldsymbol{A_{Mg}}$ is the atomic weight of the Mg^{2+} element.

Statistical Analysis

Differences of each experimental condition were evaluated by Student's t test and set as following: *p<0.05, **p<0.01.

5 RESULTS AND DISCUSSION

Part I

5.1 Cell system optimization

The first part of this study was focused on creating highly-regulated and efficient expression of *MRS2* gene.

The human embryonic kidney 293 cells[144] (HEK-293) were used as hosts for our gene of interest as they are a common model for the overexpression of recombinant proteins. The pcDNA6™/TR was used to generate a stable cell line which allowed us, in a second time, to express *MRS2* by the solely addition of tetracycline. The pcDNA6™/TR is a 6.7 kb regulator vector designed for use with the T-REx™ System. Tetracycline regulation in the T-REx™ System is based on the binding of tetracycline to the Tet repressor (TR) and derepression of the cytomegalovirus (CMV) promoter controlling expression of the gene of interest (see figure 8). [140]

Surviving cell clones of HEK-293 cell transfected with the pcDNA6™/TR, after appropriate selection with blasticidine, were picked and named Clone 2 and then used as a host cell line for our gene of interest *MRS2*.

These resulting clones were overall healthy, propagated well and exhibited normal morphology as shown in figure 6 by the comparison with HEK-293 from ATCC catalogue.

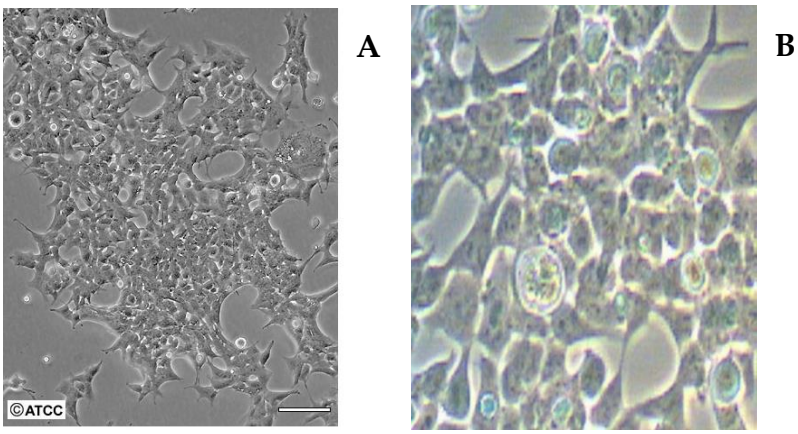

Figure 6 Morphology of (A)HEK-293 cells wild type (microphotograph obtained by ATCC) and (B) HEK-293 cells stably transfected with vector pcDNA6™/TR named Clone2. Cell morphology was observed by visible light microscopy at magnification 20x.

Firstly we performed a cell growth curves assay in order to evaluate the characteristic of cellular growth and to verify whether transfection could affected the normal cell proliferation of HEK-293 cells.

Cell growth curves allowed us to determine the best time range for testing the effects of the subsequent apoptotic inducing treatment.

Figure 7 depicts the cellular-growth curves for HEK-293 cells and its transfected counterpart with pcDNA6™/TR, Clone 2, determined by counting cells every 24 hours.

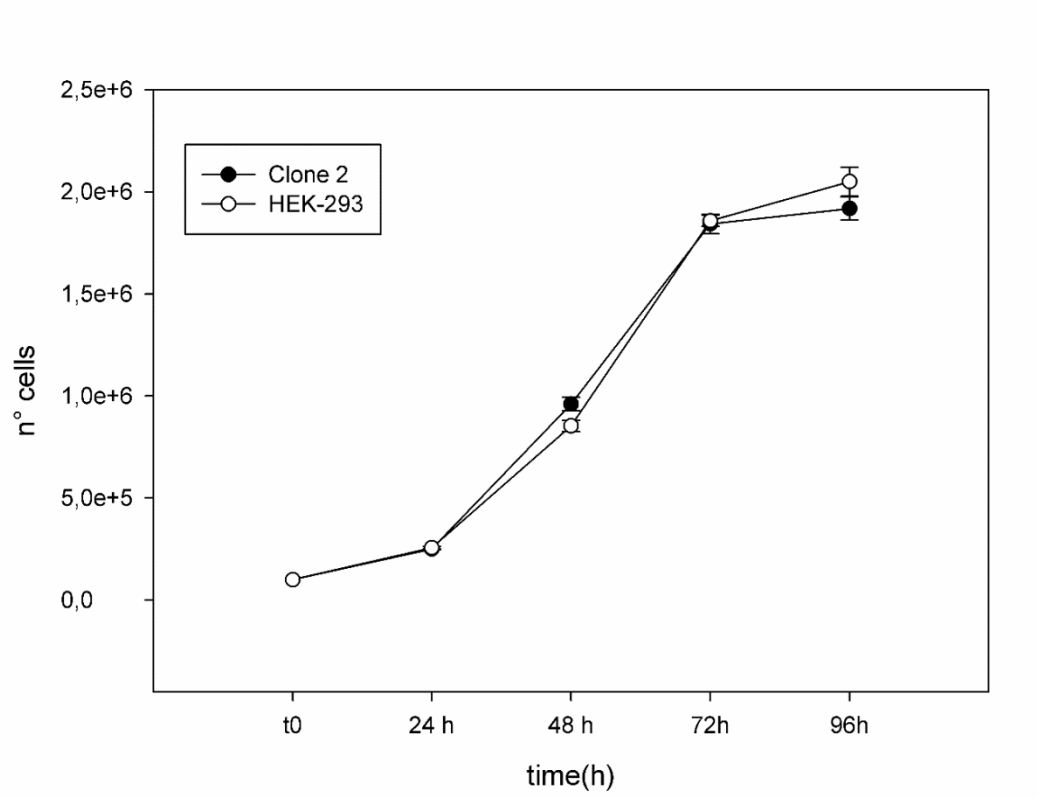

Figure 7 Cellular-growth curves for HEK-293 cells and Clone 2. Evaluation of cell number at different hours of adhesion, using a Bürker chamber. All measurements were carried out by triplicate in three different replicates.

The cell-line growth curves shows a "lag-phase" immediately after reseeding; the duration of this phase take near 24 hours.

Subsequently, the cell enter into exponential growth, "log-phase", in which the cell population doubles at a characteristic rate defined as doubling time which is characteristic for each cell line. This phase was chosen for the evaluation of drugs effects that stimulate or inhibit cell growth after MRS2 overexpression. [145]

It is possible to appreciate that HEK-293 and Clone 2 cells present the same trend as shown by doubling time, which is for both cell strains ~18hours.

5.2 MRS2 overexpression

MRS2 gene was cloned into the multiple cloning site of the inducible expression vector pcDNA™5/TO. This plasmid is a 5.7 kb expression vector specifically designed for use with the T-REx™ System and allows tetracycline-regulated expression of the gene of interest in mammalian host cells expressing the Tet repressor (TR) from the pcDNA™6/TR vector. In figure 8 are reported the plasmid maps of the two vector used for inducible expression of MRS2.

The pcDNA™5/TO vector contains hybrid promoter consisting of the human cytomegalovirus immediate-early (CMV) promoter and tetracycline operator 2 (TetO2) sites for high-level tetracycline-regulated expression.

In the absence of tetracycline, expression of the gene of interest is repressed by the binding of Tet repressor homodimers to the TetO2 sequences. Addition of tetracycline to the cells derepresses the hybrid CMV/TetO2 promoter in pcDNA™5/TO and allows expression of the gene of interest. [141]

After transfection, Clone 2 cells were treated with tetracycline 1µg/mL for 24 hours to depress the hybrid CMV/TetO2 promoter in the expression vector and induce transcription of *MRS2* gene.

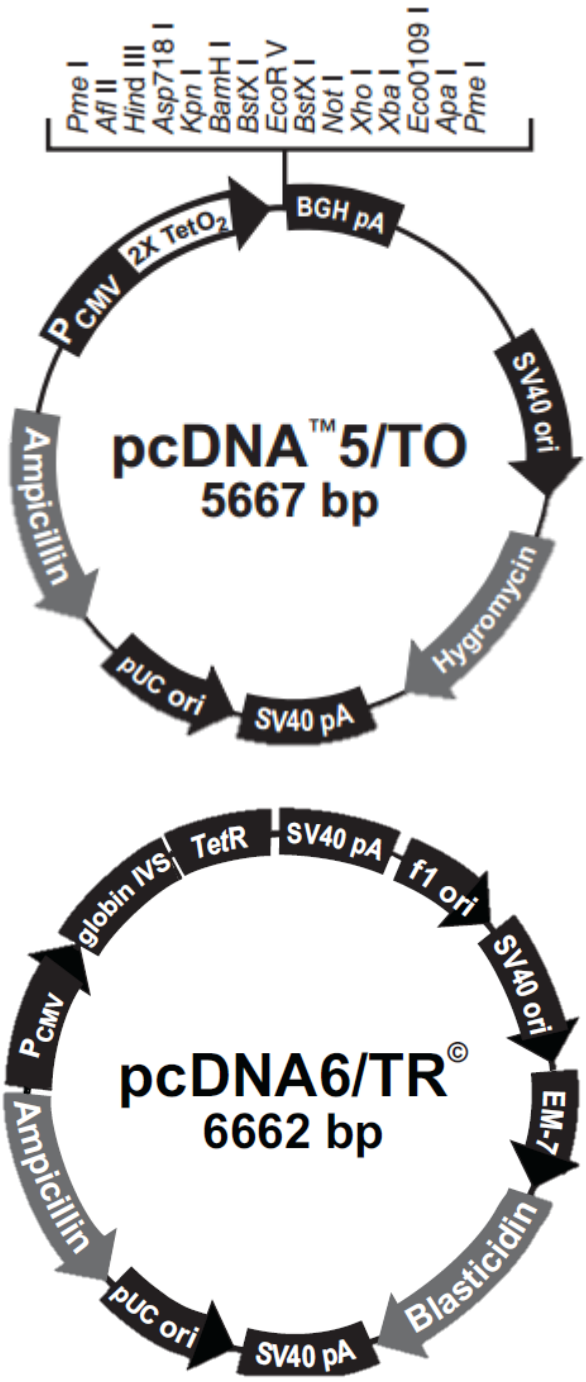

Figure 8 Plasmid maps. The two components of the tetracycline-regulated mammalian expression system (Invitrogen's T-REx™ System) used to develop the Clone2 tetracycline inducible cell line are shown. On the top, the pcDNA™5/TO expression vector with the two tetracycline operator sequences (TetO2); on the bottom, the pcDNA™6/TR regulatory vector providing high-level expression of the tetracycline repressor (TR) protein and present in the Clone 2 control cell line.

The over-expression of the channel was checked by Western Blot analysis. The cells treated with tetracycline (lane B 5-7), show higher MRS2 expression compared to un-induced control cells (lane A 1-4), as reported in figure 9. As negative control, untransfected cells has also been loaded on the gel (lane 0)

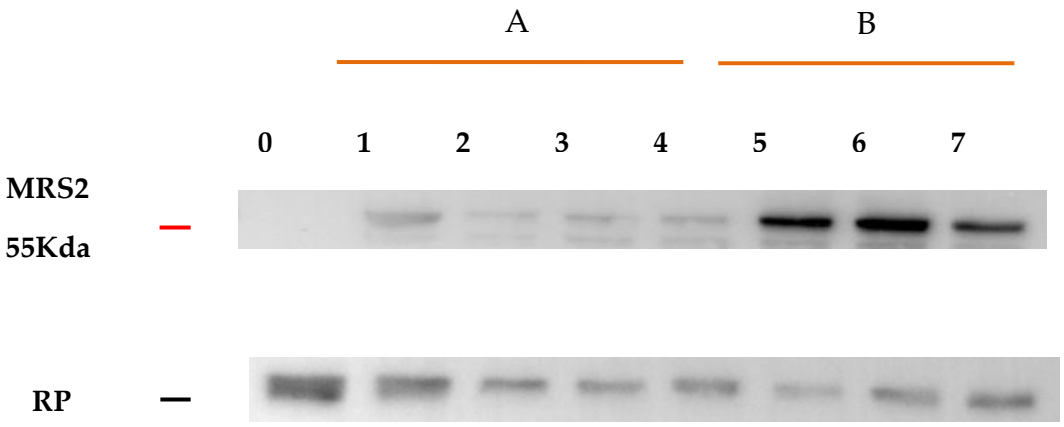

Figure 9 Comparison of MRS2 protein expression levels in the presence and absence of tetracycline 1µg/mL. Protein extracts were prepared after 24 hours from transfection with expression vector pcDNA™/5TO. (A) lane 1-4: transiently transfected Clone 2 cell line; (B) lane 5-7: transiently transfected Clone 2 cell line and induced with tetracycline resolved on reducing SDS–PAGE and analysed via Western blotting. Membranes were probed using an anti-Strep-tag-II monoclonal antibody (1:500 dilution)

MRS2 induced expression was confirmed by Immunocytochemistry: as shown in figure 10, transfection with expression vector induces highly expression of the protein localized in the perinucelar region of the cells treated with tetracycline 1µg/mL. A weak expression of the channel can also be detected in un-induced cells.

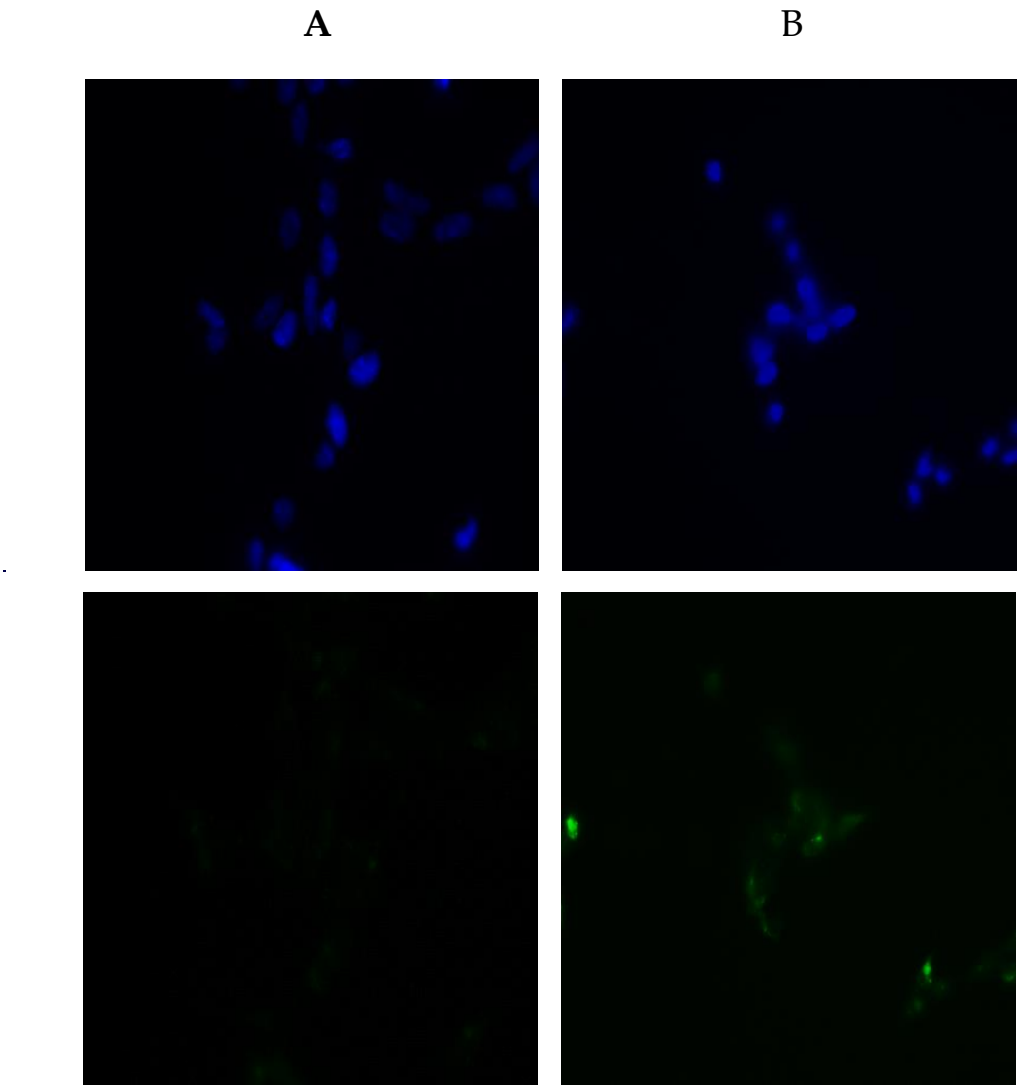

Figure 10 Morphological evaluation and expression of MRS2 in Clone 2 cells (A) and after 24 hours by induction with tetracycline 1 μg/ml (B). Double labelling immunofluorescence of nuclei stained with DAPI (upper panel) and MRS2 (lover panel) stained with Strep-tag primary antibody (1:500) and visualized with AlexaFluor-488- labeled goat anti mouse (1:500).

5.3 MRS2 is mainly expressed in the heavy mitochondrial fraction

MRS2 channel is a 55 kDa protein localized in the inner mitochondrial membrane. To examine the correct localization of the over-expressed MRS2 protein, Clone 2 induced cells were studied for subcellular fraction experiments. Nuclear fraction and debris (Fig 11A, lane1), plasma-membrane (Fig 11A, lane2), heavy mitochondrial (Fig 11A, lane3) and light mitochondrial (Fig. 11A, lane4) fractions were separated by differential centrifugation. Each of the fractionated proteins were displayed by SDS-PAGE and analyzed by immunoblotting using antibodies to the strep-tag for MRS2 (Fig 11A, top panel) and Cytochrome c oxidase (COX) protein terminal complex IV of the electron respiratory chain, as loading control for mitochondria. (Fig 11A, middle panel). In general, the heavy mitochondrial pellet contains, predominantly, mitochondria with rather few contaminants; minor components such as lysosomes, peroxisomes, Golgi membranes, and various membrane vesicles are still present. The light mitochondria pellet, contains mitochondria and other components such as lysosomes, peroxisomes, Golgi membranes and some endoplasmic reticulum.[142]

MRS2 protein was mainly found to reside in the heavy mitochondrial fraction (Fig 11B, bar 3) which is consistent with the correct localization of MRS2 in the inner mitochondrial membrane.[57]

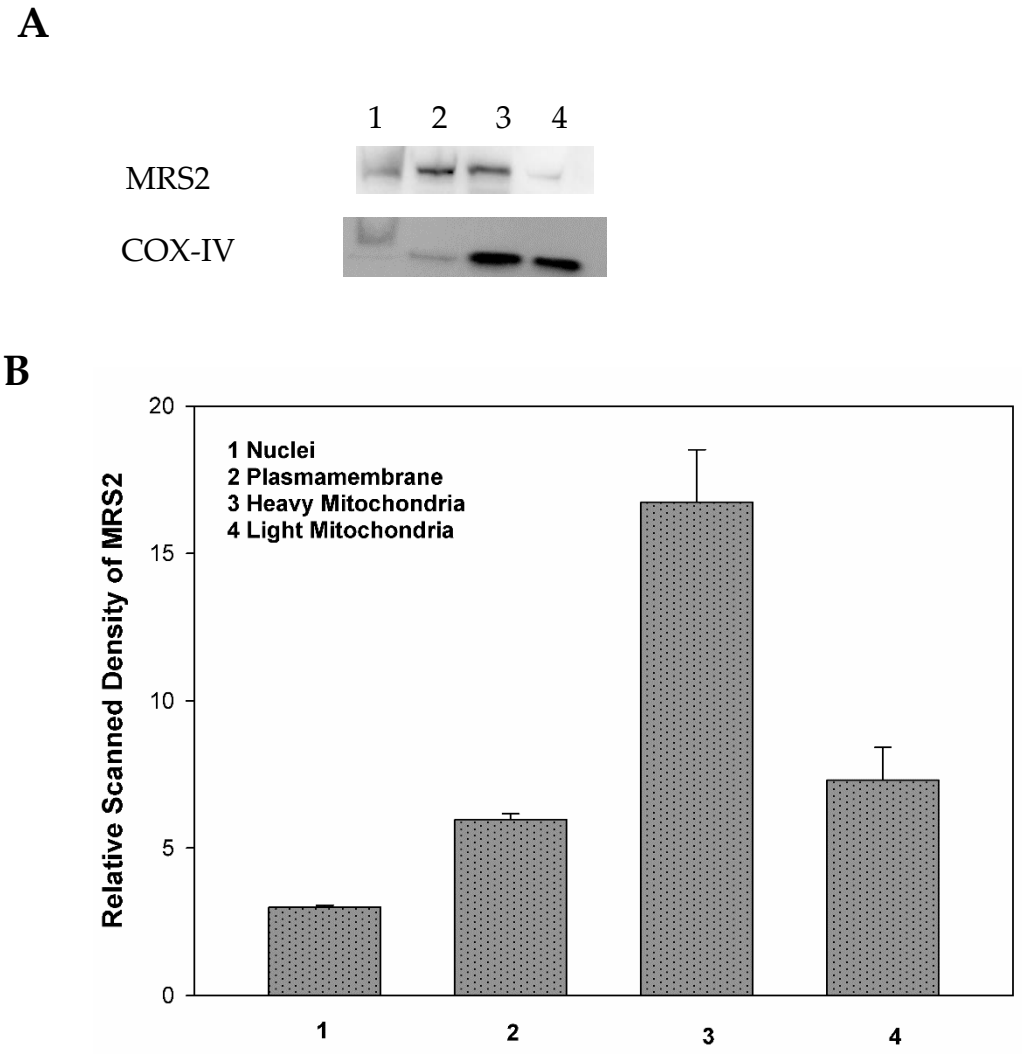

Figure 11 Isolation of human mitochondria from Clone 2 cells overexpressing MRS2
Mitochondrial fractions were obtained by differential centrifugation A) Subcellular fraction of Clone 2 overexpressing MRS2 channel. The cells were fractionated into the nuclei (lane 1), plasmamembrane (lane 2), heavy mitochondria (lane3) and light mitochondria (lane 4) fractions by differential centrifugation. Proteins were analyzed by immunoblotting using antibodies to the strep-tag MRS2 (top panel), and COX IV for effective loading control of mitochondria (bottom panel). B) Relative Scanned Density of MRS2 in subcellular fractions.

5.4 Free magnesium uptake in isolated mitochondria

Concentration of free Mg^{2+} in the matrix of mammalian mitochondria have been estimated to range between 0.2 and 1.5 mM. Since it has been published that steady state Mg^{2+} concentration of yeast mitochondria varied with the expression level of Mrs2p and that isolated mitochondria of eukaryotic cells respond to addition of external Magnesium in function of MRS2 expression, we determined changes in Mg^{2+} ion concentrations by continuous fluorescent recording over time.

By using the ion sensitive fluorescent dye membrane-permeant acetoxymethyl ester (AM) of the Mg^{2+} sensitive fluorescent dye mag-fura 2, we have performed ratiometric measurements of free Mg^{2+} concentration in isolated human mitochondria essentially following the protocol by *Kolisek et al.*[42]

Heavy mitochondrial fraction were isolated from Clone 2 cells induced and uninduced with tetracycline and transferred into a nominally Mg^{2+} -free solution for dye loading.

Figure 12 shows the ratiometric measurements corresponding to the fluorescence ratio of the original acquisition collected respectively at 340 and 380 nm excitation wavelengths which are in turn the standard excitation wavelengths for the ion-bound and free mag-fura2.

When external $MgCl_2$ was added stepwise to 1 and 3mM an increase of the fluorescent intensity ratio occurred, indicating ion passing across the mitochondrial membranes. However, mitochondrial magnesium increasing is markedly higher in cells overexpressing MRS2 channel upon addition of 3 mM $MgCl_2$.

This data is in agreement with that reported in yeast by *Kolisek et al.*, showing the capability of mitochondria to internalize Mg^{2+} by using the MRS2 channel with a rapid high capacity influx mechanism.

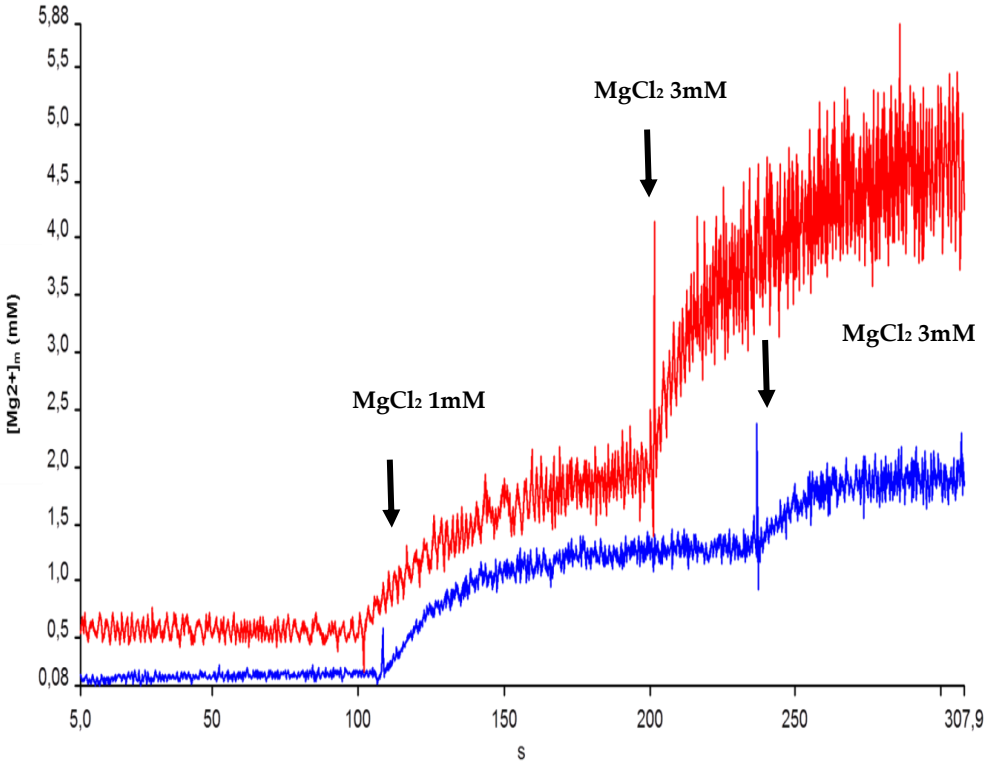

Figure 12 Determination of free Mg^{2+} in isolated mitochondria. Mitochondria isolated from Clone 2 were loaded with the Mg^{2+}-sensitive dye mag-fura 2. Changes in the free Mg^{2+} concentrations over time were determined upon raising extra-mitochondrial Mg^{2+} concentrations from nominally 0 mM to 1 mM, and from 1 mM to 3 mM. Blue line:Clone 2 control cells; Red line: Clone 2 cells overexpressing MRS2. Note the difference in the slopes of the tracings from the two mitochondria types, reflecting that Mg uptake rates depend on MRS2 expression.

5.5 MRS2 overexpression induces increment of magnesium total concentration

Total Mg^{2+} concentration is composed of a large fraction of bound Mg^{2+} and a small fraction of free Mg^{2+}. Mitochondria represent the major Mg^{2+} store in the cell and mitochondrial Mg^{2+} pools may be mobilized to buffer cytoplasmic concentration of the cation. Aimed to verify whether up-regulation of MRS2 channel could also have an influence on the intracellular total Magnesium

content we exploited the characteristic of DCHQ5, a new fluorescent chemosensor able to quantify total Mg^{2+} in sonicated cell.[113]

To express total Magnesium amount as mM concentration, we calculated the volume of Clone 2 cells.

Immediately after trypsinization, Clone 2 cells were counted and resuspended at the final concentration of 10000/mL in 20 mL final volume of PBS.

Cells were analysed by using a double-threshold Z1 Coulter Counter as reported in the "Material and methods" section and the frequency distribution of Clone 2 cell volumes is reported in figure 13. The mean cellular volume has been calculated to be 1,17E+03 fL

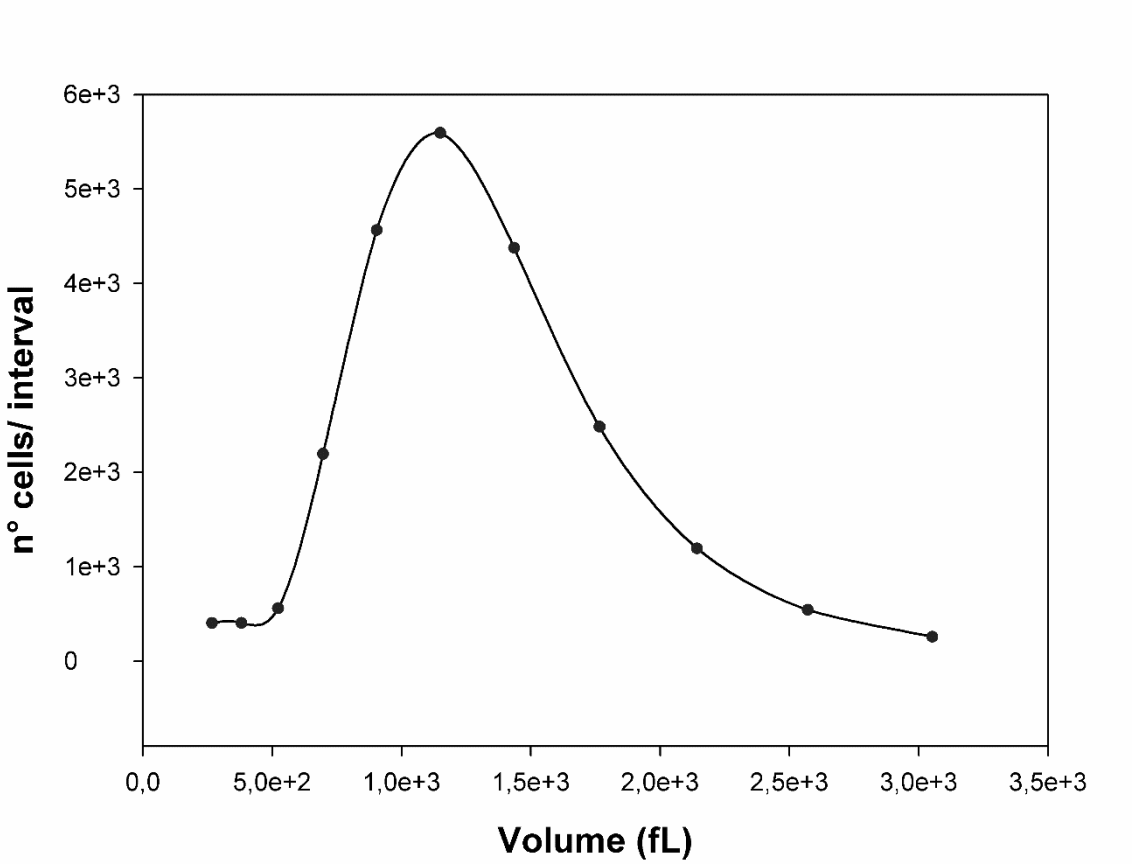

Figure 13 **Gaussian distribution of Clone 2 cells volume**.

DCHQ5 fluorescence intensity was acquired at 510 nm upon excitation at 360 nm, and the Mg^{2+} concentration of the unknown samples were obtained by the interpolation of their fluorescence with the standard curve as described in *Sargenti et al.* Measurements of total cellular Mg^{2+} revealed statistically significant increase of its concentration in clones over expressing MRS2 channel. As shown in Figure 14 total intracellular magnesium content in cells overexpressing MRS2 is 65.38±4.92 mM, three times more than in control cells, which present an average concentration of 22.47±2.03 mM.

Quantification of total intracellular Mg^{2+} by using DCHQ5 allowed us to reach unprecedented result and to demonstrate for the first time that MRS2 protein overexpression is able to induce an increment of the total intracellular Mg^{2+} in human cells. We hypothesize that this increased amount of magnesium is due to the high capability of MRS2 to retrieve Mg^{2+} in mitochondria.

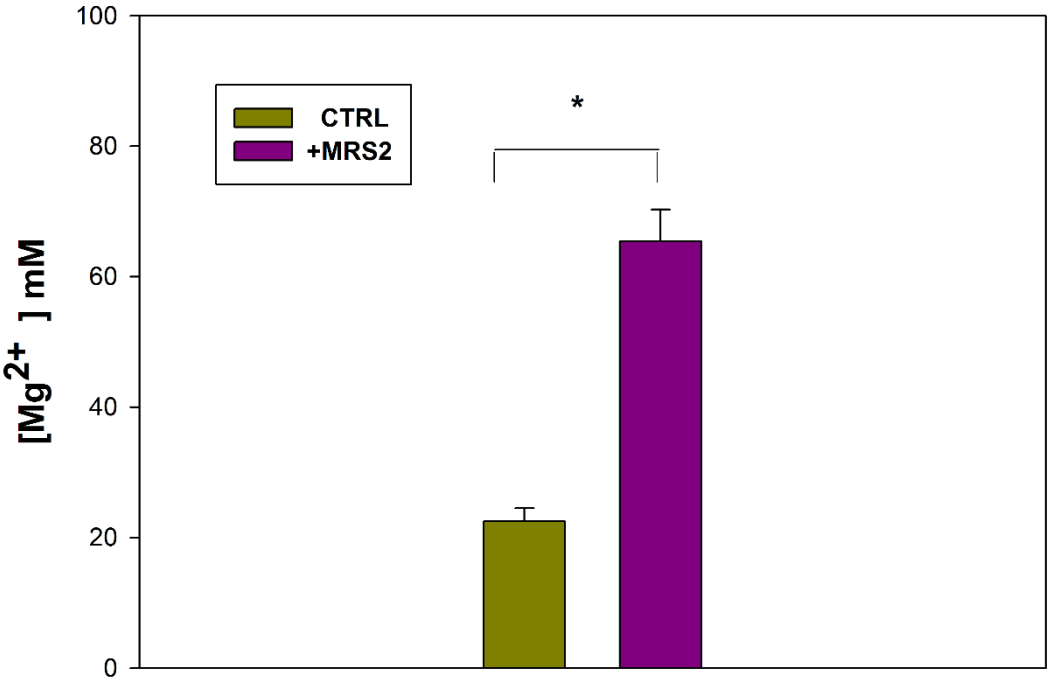

Figure 14 Fluorimetric analysis of total magnesium content in Clone 2. Measurement were carried out in sonicated sample by using the fluorescent probe DCHQ5 in Clone 2 cell control (CTRL) and overexpressing MRS2 protein (MRS2).

5.6 MRS2 overexpression protects from apoptotic stimuli

Many aspects of Mg^{2+} biochemistry indicate a role for this cation in the apoptotic process sustained by the fact that mitochondria which are the key organelle in the onset of apoptotic programme are the main intracellular Mg^{2+} store.[87]

In particular, it has been proposed a link between apoptosis and Mg^{2+} mitochondrial channel MRS2. MRS2, by promoting Mg^{2+} uptake, potentiates mitochondrial energetic function, which sustains both pump activity, by Mg^{2+}-ATP^{2-}, and cell proliferation.

To verify this hypothesis we induced cell death in Clone 2 cells overexpressing MRS2 protein by two common pro-apoptotic drug stimuli: doxorubicin (DXR) and staurosporine (STS)

5.6.1 Effect of MRS2 overexpression during DXR induced apoptosis

Doxorubicin is a well-known chemotherapeutic agent used in treatment of a wide variety of tumours. Its interaction with cellular DNA along with apoptosis activation via intrinsic pathway is believed to be the principal mechanism of its biological activity. [146]

The ability of doxorubicin to affect cell viability and apoptosis induction was initially confirmed by morphological evaluation. After incubation with DXR 2.5μM for 17 h, morphological alterations in Clone 2 cells, induced and uninduced with Tet, were observed in bright field in comparison to control cells. As shown in figure 15, control cells showed their typical morphology, appearing adherent to the tissue culture dishes and with several nucleoli. In contrast, exposure of Clone2 cells treated with DXR revealed typical apoptotic

features such as rounding, shrinkage and losing contact with adjacent cells. Finally, DXR treatment on the cell induced with tetracycline 1µg/mL and overexpressing MRS2 channel present more similar morphology to untreated cells with more adherent cells to the culture dishes and rare rounding cells.

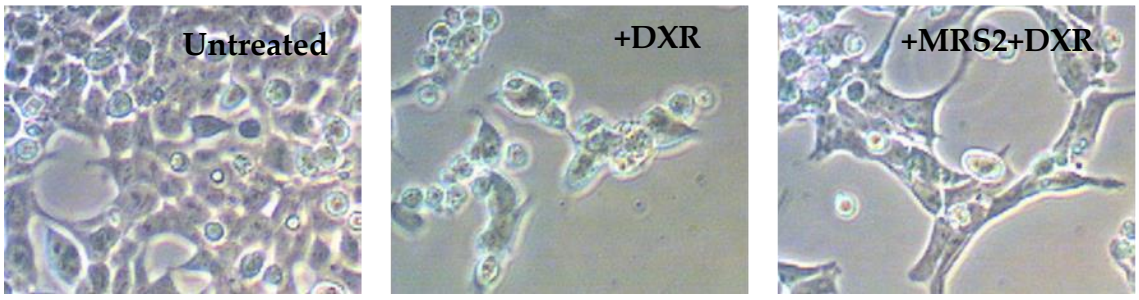

Figure 15 Morphological evaluation of Clone 2 cells treated with DXR
Clone 2 cells, induced(+MRS2+DXR) and un-induced (DXR) with Tet were treated with DXR 2.5µM for 17 hours after induction. Untreated cell is also show as control.

Clone 2 cells, were subjected to fluorescence microscopy evaluation by staining nuclei with Hoechst 33342 to check the presence of nuclear condensation and DNA fragmentation typically occurring in apoptosis. Coverslips with adherent Clone 2 and treated with DXR 2.5µM after 17 hours were fixed with 3.7% paraformaldehyde and stained with Hoechst 33342 (1 µg/ml).

As depicted in figure 16, the untreated control cells displayed normal, round nuclei (CTRL) as well as MRS2 overexpressing cells treated with DXR(+MRS2+DXR), while Clone2 cells treated with DXR exhibited characteristics of apoptosis, such as cell shrinkage and nuclear condensation (DXR).

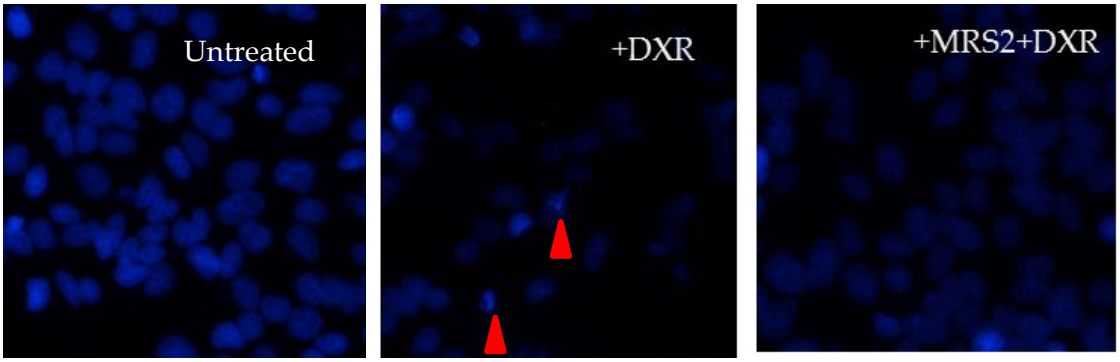

Figure 16 Morphological evaluation of DNA fragmentation and Chromatin condensation of Clone 2 cells after treatment with DXR upon MRS2 overexpression. Clone 2 cells Control (CTRL), treated with doxorubicin 2.5μM (DXR) and Clone 2 overexpressing MRS2 channel treated with doxorubicin 2.5μM (+MRS2+DXR) were grown on glass coverslips, and detached 17 hours after treatment.
Cells were fixed with paraformaldehyde 3.7% and nuclei were stained with Hoechst 33342 and subjected to fluorescence microscopy. Images reported are from one experiment representative of three that gave similar results.

Since it is largely known that doxorubicin treatment affects cell cycle progression we investigated whether the MRS2 expression could also have an influence on DNA content during apoptosis induction by DXR.

To accomplish this task we choose two different DXR concentration as it is reported that effect of DXR on cell cycle is highly dependent on the dose of treatment.[147]

Clone 2 cells control and overexpressing MRS2 channel were exposed to doxorubicin 2.5 and 5 μM As shown in figure 17 A both doses of doxorubicin affect cell cycle progression of Clone 2. The lower dose of 2.5 μM induces a remarkable increase in cells residing in S to G2-M phase. The increased dose DXR(5 μM) resulted in a depletion of cells in S to G2-M phase that can be explained by a massive apoptosis in particular in these phases.

As the apoptotic cells with fragmented nuclei appear as cells with hypodiploid DNA content and could be detected at sub-G1 peak with flow cytometry, the numbers of the apoptotic sub-G1 population were quantified.

The results demonstrated that the DXR treated Clone2 samples had significantly increased in the sub-G1 phase as compared to the untreated sample and to sample treated but overexpressing MRS2.

Furthermore, in control cells the sub-G1 populations increased in dose dependent way, from 3,09 % in untreated cells to 16.47 % and 76.74% respectively in cells treated with 2.5 μM and 5 μM DXR.

On the contrary, in cells over-expressing MRS2 the influence of doxorubicin on cell cycle is very weak and minor dependent of the dose (figure 17 B) We can observe a slight increase of cells in the S and G2/M phase when these cells were treated with 2.5 DXR. However, this weak effect disappear at the highest dose of 5 μM which did not induce variation of DNA content respect to untreated cells.

These results indicate that apoptosis is the cell death mode of DXR in Clone 2 cells and most of all that MRS2 prevent from this drug effect on cell cycle progression.

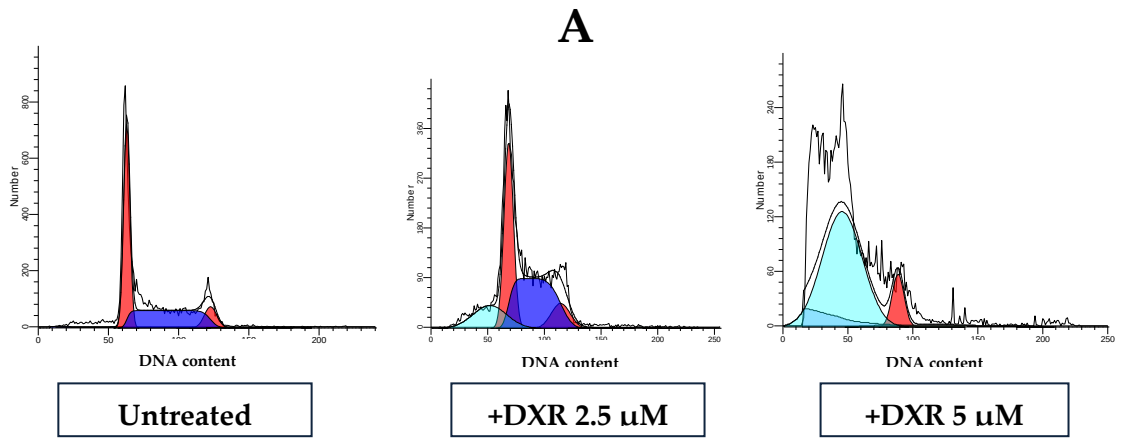

Table II Percentage of cells cycle distribution in Clone 2 cells treated with DXR 2.5 and 5µM.

	G0/G1%	S%	G2/M%	Apoptosis
	51.24	36.38	11.9	3.09
2.5µM	41.57	49.20	9.23	16.47
5µM	100			76.74

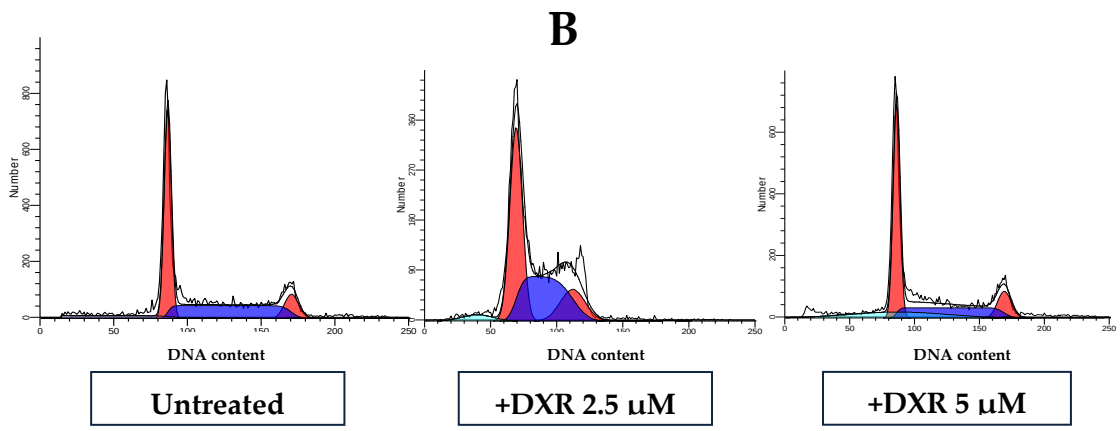

Table III Percentage of cells cycle distribution in Clone 2 cells overexpressing MRS2 channel treated with DXR 2.5 and 5µM.

	G0/G1%	S%	G2/M%	Apoptosis
	48.99	41.65	9.36	2.41
2.5µM	46.22	36.38	15.10	3.71
5µM	45.38	44.084	10.548	6.3

Figure 17 Flow cytometric analysis of Clone 2 (A) control cells and (B) overexpressing MRS2 channel. treated with doxorubicin (DXR). Cells were harvested at 17 h after 2.5 and 5 µM DXR treatment and collected in a citrate buffer. Then, RNA was digested and DNA content was stained with propidium iodide(PI). Cell cycle distribution was determined by flow cytometry. The histograms reports DNA content (expressed in fluorescence channels) versus the number of acquired events. DNA content is directly proportional to PI fluorescence.

Apoptosis is a process of active cellular self-demolition that requires the expression of specific genes. Despite the diversity of signals that can induce cell death, these pathways share several features in their execution. One mechanism, which is consistently implicated in apoptosis, reflects an orchestrated series of biochemical events that is carried out by a group of cytosolic proteases, named caspases. Activation of these protein is considered one of the hallmark of triggered apoptosis. Thus, inhibition of the activity of caspase-3 might protect cells from apoptosis.

We tested the activity of executioner caspases in order to demonstrate that MRS2 truly prevent from DXR cell death induction. In particular we evaluated the DEVDase activity of caspase 3/7 after treatment with DXR 5 μM .

As expected, DXR significantly increased caspase activity in control cells.[146] On the contrary, MRS2 overexpressing cells respond to DXR exposure with a lower activation of these proteins. (Figure 18)

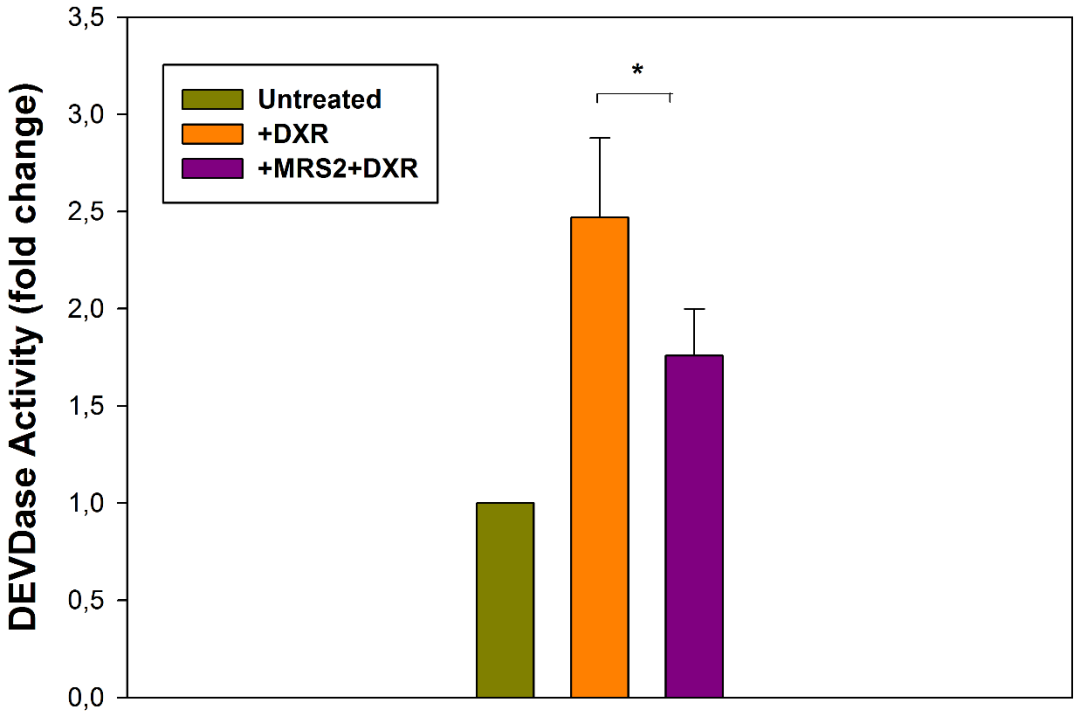

Figure 18 Caspase Activity assay. The activity of caspase proteases (DEVDase activity) was measured fluorimetrically in Clone2 cells control and overexpressing MRS2 channel after treatement with 5μM DXR for 17 h. * Indicate significantly difference $P < 0.05$

5.6.2 Effect of MRS2 overexpression during STS induced apoptosis

Staurosporine is a strong inhibitor of Protein kinase C widely used as therapeutic agent in tumour treatment for its ability to activate intrinsic apoptotic pathway. [148]

We used this drug as established known inducer of apoptosis to confirm the results previously obtained with DXR.

Clone 2 cells were treated with STS 2 μM and after 6 hours of treatment were analysed by fluorescence microscopy to evaluate the typical morphological changes of apoptosis such as reduction of cell volume and nuclear fragmentation

As illustrated in Figure 19, Clone2 cells incubated with STS exhibited many more cells with condensed and fragmented nuclei than those treated with STS and overexpressing MRS2 channel. This latter appear more similar to untreated cells.

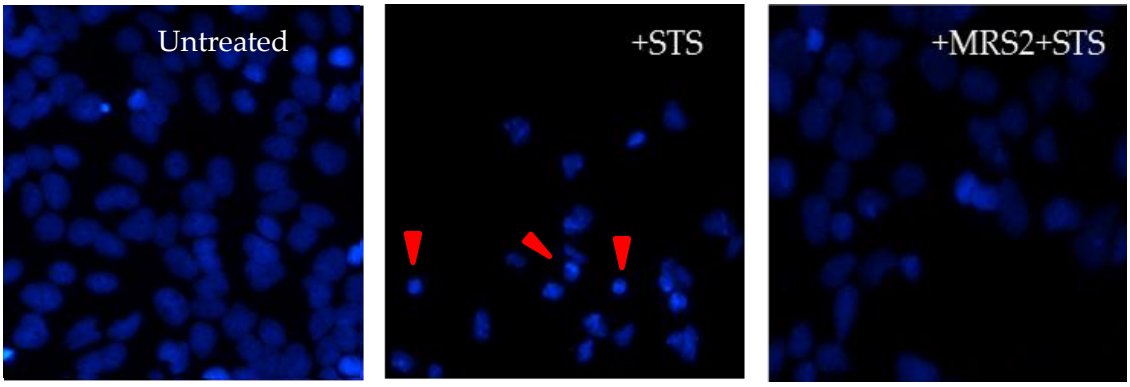

Figure 19 Morphological evaluation of DNA fragmentation and Chromatin condensation of Clone 2 cells after treatment with Staurosporine (STS) upon MRS2 overexpression.
Clone 2 cells Control (CTRL), treated with STS 2μM (STS) and Clone 2 overexpressing MRS2 channel treated with staurosporine 2 (+MRS2+STS) were grown on glass coverslips, and after6 hours after treatment. Cells were fixed with paraformaldehyde 3.7% and nuclei were stained with Hoechst 33342 and subjected to fluorescence microscopy. Images reported are from one experiment representative of three that gave similar results.

To further investigate the STS triggered apoptosis upon MRS2 overexpression, Clone2 cells were then subjected to flow cytometric analysis.

In particular, we monitored the effect of staurosporine on cell cycle distribution. Indeed, the predominant effect of staurosporine is to induce block of cell cycle in the G2/M phase.[148]

Effects of staurosporine were detected by comparing the cell cycle profiles between treated and untreated cells. Results, showed in figure 20 A, demonstrates a decrease of the G0/G1 phase with a concomitant increase in the G2/M phase in treated cells. Moreover, the sub-G1 peak is detectable. These results confirmed the cell cycle arrest at the G2/M checkpoint as the major effect of this molecule on DNA content and the triggering of apoptosis evidenced by sub-G1 peak. The percentage of cells in the S, G1, and G2/M phases are shown in Table IV.

In figure 20 B are reported cell cycle profile of Clone 2 cells overexpressing MRS2 treated and untreated with STS 2 μM. Notably, cells do not show the typical G2/M arrest induced by this drug, but even the G0/G1 phase is more pronounced respect to untreated cells with ~71% of cells in this phase.

This result evidence that STS may affect cell cycle in MRS2 positive cells with a less extent and by a different mechanism. Furthermore, this data would be fitted in the complex network of cellular signals and give an indirect insight into the relationship between Magnesium and protein kinase C. Indeed, the main pathway for Mg^{2+} accumulation in mammalian cells is the activation of protein kinase C (PKC). Moreover it has been shown that the neuroprotective role of Magnesium against damage to synaptic transmission may include altering the PKC response to anoxic insults. It seems that magnesium induce the translocation of PKC to the membrane cytoskeleton and to augment its activity.[149]

A

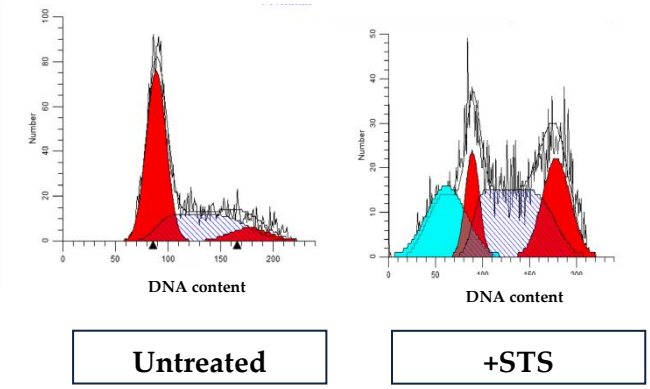

Table IV Percentage of cells cycle distribution in Clone 2 cells treated with STS 2μM.

	G0/G1%	S%	G2/M%	Apoptosis
	58.30	26.14	15.56	
2 μM	16.47	31.32	51.95	24.15

B

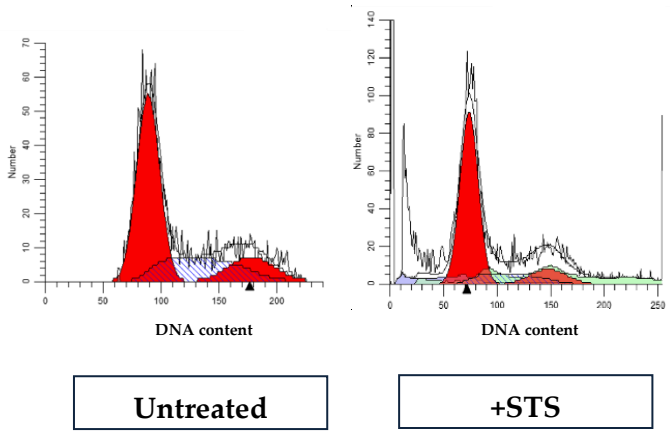

Table V Percentage of cells cycle distribution in Clone 2 cells overexpressing MRS2 channel treated with STS 2μM.

	G0/G1%	S%	G2/M%	Apoptosis
	56.65	34.54	8.81	
2 μM	72.55	12.55	14.79	0.13

Figure 20 Flow cytometric analysis of Clone 2 (A) control cells and (B) overexpressing MRS2 channel. treated with staurosporine(STS). Cells were harvested at 6h after 2 μM STS treatment and collected in a citrate buffer. Then, RNA was digested and DNA content was stained with propidium iodide. Cell cycle distribution was determined by flow cytometry. The histograms reports PI fluorescence (expressed in fluorescence channels) versus the number of acquired events. PI fluorescence is directly proportional to DNA content.

To deepen the effect of staurosporine on Clone 2 cells overexpressing MRS2 channel we evaluate the activity of executioner caspases-3/7 after treatment with STS.

Our results reveals an increased caspase activity in control cells after exposure with staurosporine 2 μM. Although with a less extent, respect to DXR treatment, MRS2 overexpression induce a less responsiveness of executioner caspases upon staurosporine treatment. (Figure 21)

Since MRS2 overexpression seems to interfere with the caspase-3/7 activity in the Clone 2 cells, it has the capacity to attenuate the effect of STS induced apoptosis.

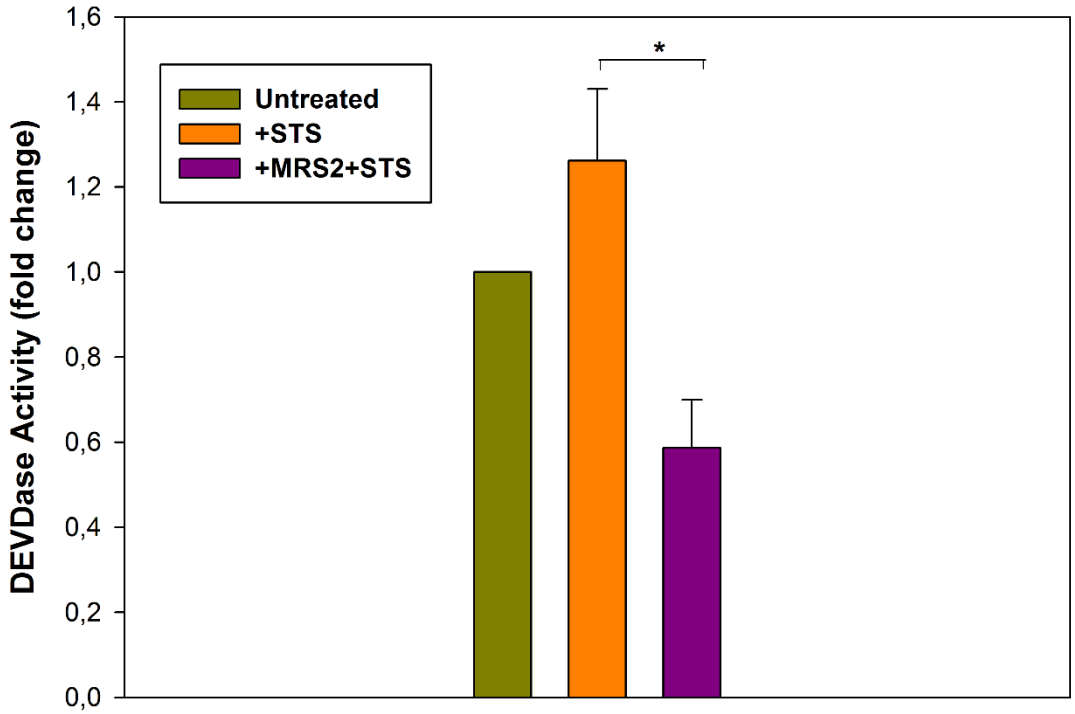

Figure 21 Caspase Activity assay. The activity of caspase proteases (DEVDase activity) was measured fluorimetrically in Clone2 cells control and overexpressing MRS2 channel after treatement with 2μM STS for 6 h.* P<0.05

Part II

Basic and pre-clinical studies indicate that a relationship between magnesium and cancer exists and that magnesium deficiency can have both anti- and pro-tumour effects. [99] In particular, recent evidences pointed out a role for Mg^{2+} in resistance of cancer cells to antitumor drugs. The acquired resistance to a single anticancer agent is frequently accompanied by the development of cross-resistance to multiple drugs. This phenomenon, known as MDR appears to be due to a reduced net intracellular drug accumulation resulting from overexpression of specific protein acting as efflux pumps. [106]

Considering the established role of Mg^{2+} in cell metabolism its deregulation in cancer cells is reflected into impaired intracellular Mg^{2+} concentration, compartmentalization and distribution potentially leading to MDR phenotype.

In the second part of this research, we aimed to verify if intracellular Mg^{2+} content could be used as a feature to distinguish MDR cell phenotype from their sensitive counterpart.

5.7 MDR cell phenotype

Firstly we performed a cell growth curves assay to compare cellular growth of the two cellular strains understudy: colon adenocarcinoma cell line sensitive (LoVo-S) and resistant to doxorubicin (LoVo-R). Resistant cells were growth retarded when compared to sensitive ones (Fig. 22A). In particular, while LoVo-S started to double 24 hours after seeding, LoVo-R entered the exponential phase after 48 hours. These results were further investigated by analyzing cell cycle distribution by flow cytometry . Figure 22B shows that the percentage of LoVo-S in the S phase started to decrease at 96 h, after reaching confluence. On

the contrary, in LoVo-R the S phase was still maximal after 96 hours from seeding and began to decrease only at 168 hours (Fig. 22B). Thus, the amount of cells in S phase directly correlates with the proliferation rate of the two cell lines.

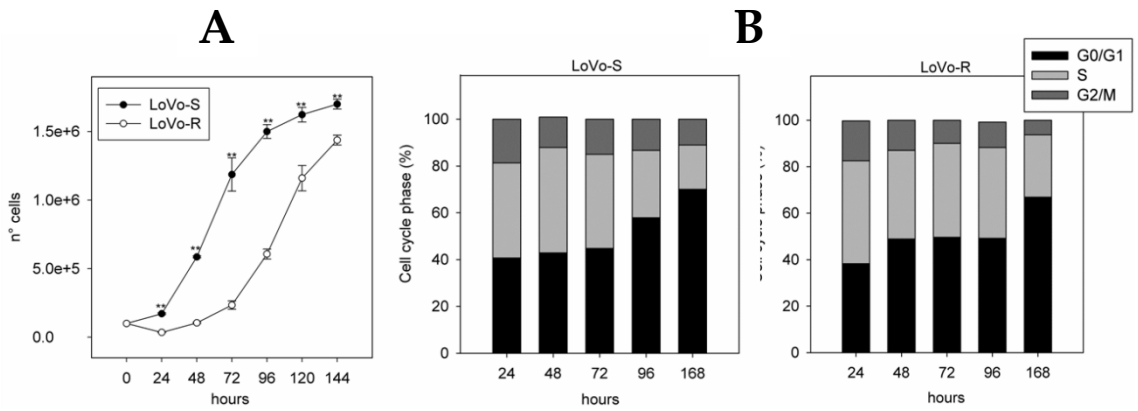

Figure 22 Comparison of cellular growth curve(A) and cell cycle analysis(B) of LoVo-S and Lovo-R cells. Evaluation of cell number at different hours of adhesion, using a Bürker chamber. All measurements were carried out by triplicate in three different replicates.Cell cycle analysis were carried out by using flow cytometer. Both cell strains incubated with the DNA-staining chemical propidium iodide for DNA content-based assessment of cell-cycle distribution.

5.7.1 Magnesium intracellular concentration is higher in resistant cells

It is well known that tumour cells present the peculiarity to accumulate Mg^{2+} with higher extent respect to non-tumour cells.[13] To characterize Mg^{2+} profile of LoVo cells, we analyzed the intracellular magnesium content in viable cell by using DCHQ5 chemosensor. DCHQ5 belongs to a family of fluorescent hydroxyquinoline derivatives showing a remarkable affinity and specificity for magnesium, higher than the other commercially available probes.

In particular, this probe allows a versatile flow cytometric semi-quantitative determination of total magnesium concentrations in whole cells, being excited in UV and the visible field. Furthermore, DCHQ5 chemosensor allows multiparametric analysis beings capable to selectively stain live cells and

resulting well tolerated by the cells at loading concentration of 5µM and incubation time up to 30 minutes.[150]

LoVo-S and LoVo-R cells loaded with DCHQ5 and counterstained with PI were analysed by flow cytometry to discriminate live from damaged cells and selectively analyse intracellular Mg^{2+} content.

Figure 23 reports the cytograms of LoVo cells: PI positive/damaged cells (quadrant A) are distinct from DCHQ5 fluorescent cells (quadrant D), suggesting that DCHQ5 selectively stains live cells.

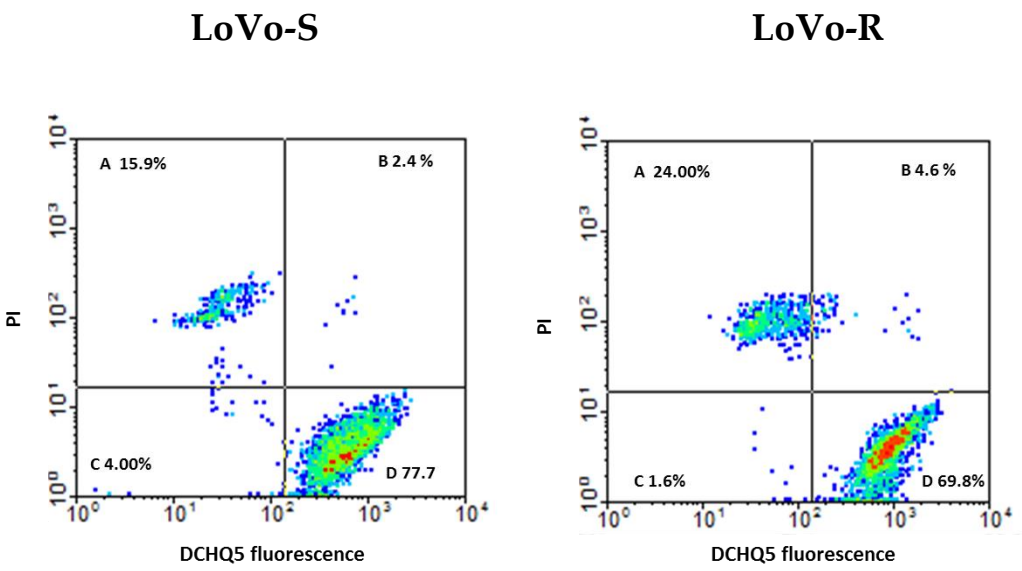

Figure 23 Cytograms of LoVo S (left) and LoVo-R (right) cells loaded with DCHQ5 and PI analysed after 15 min of incubation at room temperature. Quadrant A: PI positive/damaged cells with low DCHQ5 fluorescence; quadrant C: PI negative/viable cells with low DCHQ5 fluorescence; quadrant D: PI negative/viable cells with high DCHQ5 fluorescence. The percentage of cell population is indicated in each quadrant. Cells were resuspended at the concentration of 5×10^5/ml; DCHQ5 5 µM; PI 5µg/mL. Results from a typical experiment repeated three times with similar results

Our data shows a different fluorescence intensity of DCHQ5 in live cells pertained to the two cell strains, indicating that LoVo-R cells present higher Mg^{2+} amount.

Magnesium levels were then correlate with cell dimension by integrating DCHQ5 fluorescence intensity of live cells to forward scattering signal (FS). Cell dimension was estimated by detecting forward scattered light in the direction of the laser path and analysing the signal.

Histograms of DCHQ5 fluorescence and of FS of LoVo sensitive and resistant cells are showed in figure 24.

Analysis of the aforesaid histograms are reported in table VI: LoVo-R present higher Mg^{2+} content compared to LoVo-S cells presenting a mean channel for DCHQ5 fluorescence of 864.03 respect to 698.11.

Although LoVo-R cells show higher Mg^{2+} levels than LoVo-S cells their dimension seems to be reduced displaying a FS mean intensity channel one third slighter compared to LoVo-S cells.

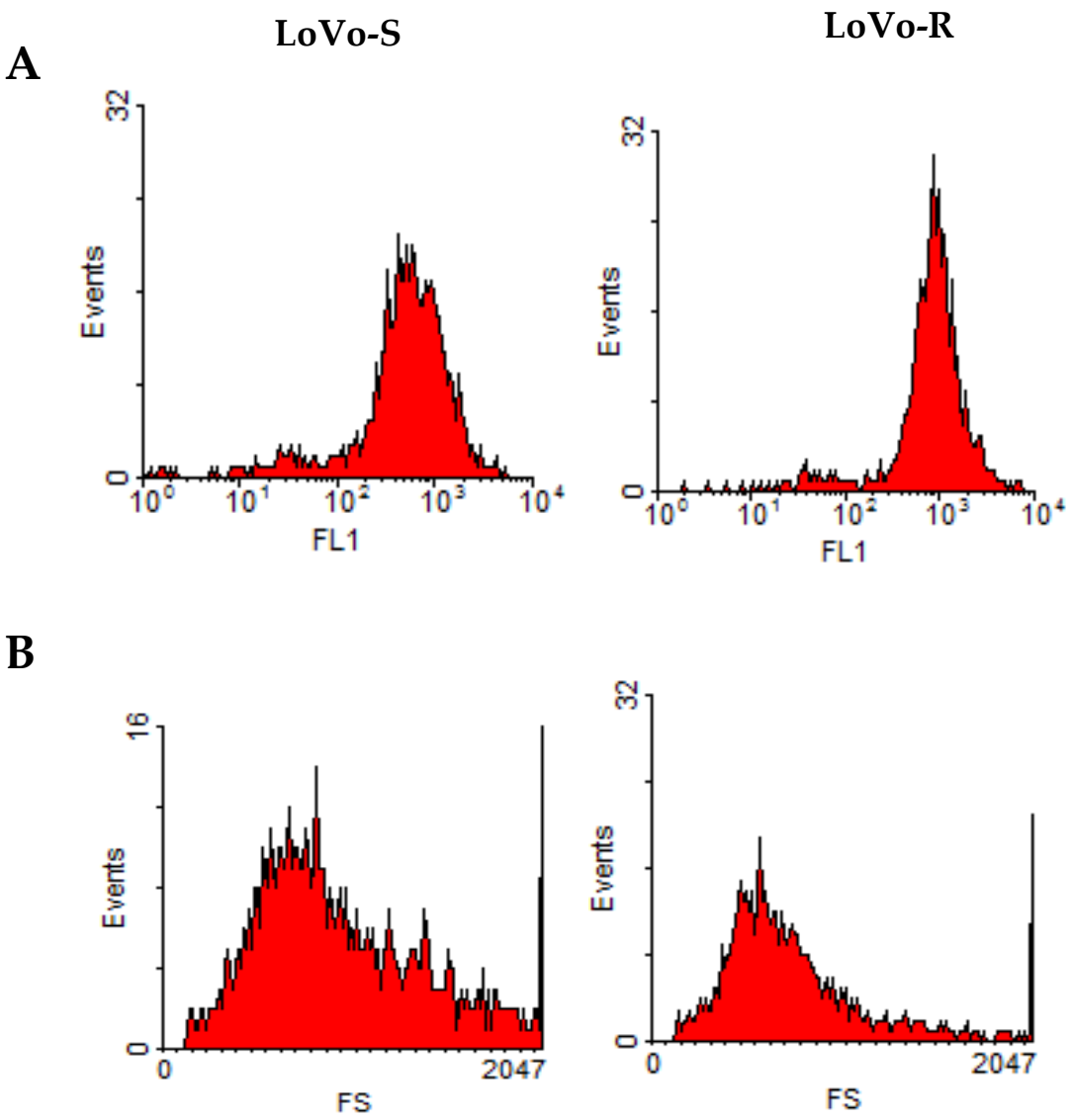

Figure 24 Cytograms of LoVo S (left) and LoVo-R (right) cells. In the upper panel (A) are reported the flow cytometric histograms of LoVo-S and Lovo R cells stained with DCHQ5 5μM to evaluate Mg intracellular levels. In the lower panel (B) are reported representative FACS histogram showing Forward Scattering (FS) of LoVo-S and Lovo-R cells. Forward light scatter was considered a function of cell size. Typical histograms of at least three independent experiments.

Table VI Mean channel of FS and DCHQ5 fluorescence in LoVos and LoVo R cells.

Taking into account the information given by flow cytometric analysis, we performed quantitative spectrofluorimetric assay with DCHQ5 in order to quantify the total Mg^{2+} concentrations in a large cell population. As expected for hydroxyquinoline derivatives, DCHQ5 fluorescence is affected by membrane-defined intracellular compartments.[114] In order to prevent false positive of fluorescence intensity due to the interference of lypophilic structure of the cellular membranes, the cells were exactly counted and sonicated prior to perform the fluorimetric assay.

Furthermore, we calculated the exact volume of LoVo-S and LoVo-R cells by using Beckman coulter counter because Mg^{2+} intracellular concentration is significantly influenced by cell dimension.

As shown by Gaussian distribution of cell volumes, represented in figure 25, sensitive cells are bigger respect to resistant cells. Moreover, while the volume of LoVo-R cells present a typical Gaussian distribution with mean calculated value of 1380 fL, LoVo-S cells are more homogeneous presenting a large part of the analysed population with high ratio for number of cells per interval. In this case the mean cellular volume has been calculated to be 1600 fL.

	FS mean channel	DCHQ5 mean channel
LoVo-S	920.22	541.98
LoVo-R	698.11	864.03

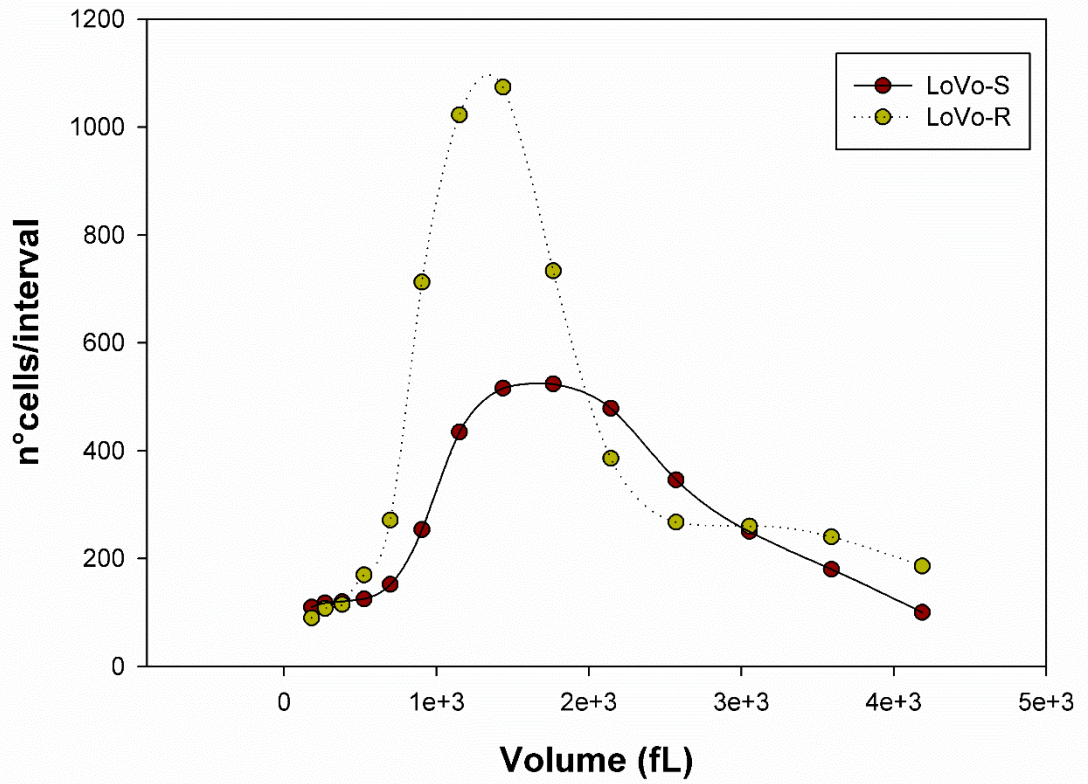

Figure 25 Gaussian distribution of LoVo –S and Lovo-R cells.

Therefore, we normalized the amount of magnesium assessed by fluorimetric assay to the calculated cells volume, thus providing molar concentration of total intracellular Mg^{2+}.

Histogram reported in figure 26 represents the total intracellular magnesium concentrations in the two cell strains after 24 hours of adhesion. Resistant cells contain statically significant more total Mg^{2+} concentration than sensitive cells presenting an average concentration of 24±2.03 mM compared to 19.10±1.45 mM of LoVo-S cells.

This result is in agreement with that reported by *Marverti et al.* founding increased amount of Mg^{2+} in cis-platin resistant human ovarian carcinoma cell line (C13*) compared to sensitive cells.[112] This difference can attributed to a different expression pattern of Mg^{2+} transporters. In particular, the mitochondrial Mg^{2+} transporter MRS2 has recently gaining increasing attention for its involvement in MDR cell phenotype. Since an up-regulation of this

channel has been found in gastric cancer cells resistant to doxorubicin it would be interesting to investigate whether it has different expression also in LoVo R respect to LoVo-S cells.

It is worth noting that our obtained data refers to the time in which the cells have adhered and are beginning to proliferate.

Role of Mg^{2+} in regulating cell proliferation is well established. Coherently with the promoting role of Mg^{2+} on protein and DNA synthesis, proliferating cells contain more Mg^{2+} than resting ones and require appropriate Mg^{2+} level to occur.

Among Mg^{2+} transporters, Transient Receptor Potential Melastatin 7 (TRPM7) channel, has reported to regulate cell proliferation and invasion of cancer cells. Although TRPM7 represents the major magnesium-uptake mechanism in mammalian cells and its over-expression has been found in a variety of human carcinoma cells, no data are available about the expression of TRPM7 in drug resistant tumour cells so far.[50] However, unpublished data of our collaborators indicate a different expression of TRMP7 channel in colon cancer LoVo cells sensitive and resistant to doxorubicin.

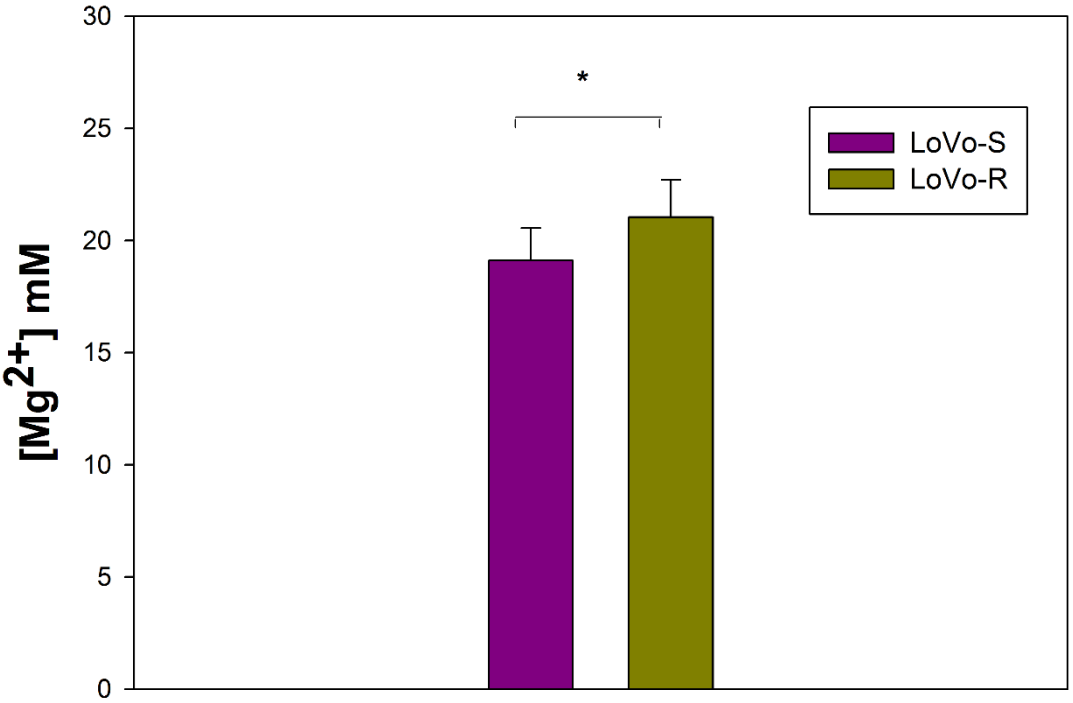

Figure 26 Total Mg^{2+} concentrations of LoVo-S and Lovo-R cells. Magnesium intracellular concentration was evaluated fluorimetriccly by using DCHQ5 chemosensor in sonicated samples. * Indicate a P value ~ 0.02

5.7.2 Different magnesium intracellular distribution pattern in drug-sensitive and -resistant cells

With the continuous development of analytical techniques providing complex information at single cell level, the study of cell heterogeneity has been the focus of several research projects within analytical biotechnology.

However, in Mg^{2+} field there is a lack of information about the exact intracellular concentration and distribution of this element.

By adopting a multidisciplinary approach, with the use of complementary techniques and implementation of custom-made algorithms, we reached the challenging issue to obtain molar concentration maps of Mg^{2+} in whole single cell. To do this we combined Atomic Force Microscopy (AFM), with synchrotron based X-ray fluorescence Microscopy (XRFM) and Scanning

Transmission X-ray Microscopy (STXM), in Lovo-S and LoVo-R fixed cells. Atomic Force Micrsocopy measurements gave us morphology information (thickness) providing the volume of each single cell analysed. The volume of the dehydrated cells has been estimated 166 fL for LoVo-S cells and 142 fL for LoVo-R cells. The merger of all of these techniques (multimodal fusion approach) permits to have all the information necessary to draw the intracellular elemental maps of mass fraction and molar concentration of Mg^{2+} (Figure 27). In particular, molar concentration distribution were obtained by normalizing the maps of fluorescence intensity respectively to volume maps (see eqs 2 and 3 of Materials and Methods). This accurate approach provides both submicrometer spatial resolution and quantification of elements down to 10^6 atoms/ μm^3 (based on the minimum Mg^{2+} concentration detected in a single pixel, i.e., 1 mM).

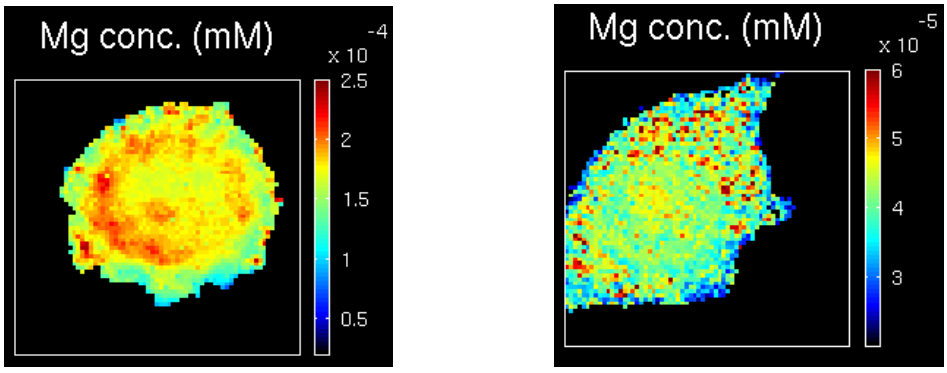

Figure 27 Morphology and concentration map human of colon carcinoma LoVo-R (left) and LoVo-S (right). Total Mg^{2+} concentration maps evaluated by matching AFM, XRFM and STXM given information.

It is worth noting that the comparison between LoVo-R and LoVo-S cells revelead different patterns in the spatial distribution of Mg^{2+} concentration. LoVo-R cells present the highest values of molar concentration within the nucleus and in the perinuclear region, where most of intracellular organelles

and particularly mitochondria, are located. This is in agreement with the experimental evidences that mitochondria are the major intracellular magnesium stores inside the cells.

On the contrary, LoVo-S cells showed the highest value in the cytoplasmic periferal region. It can be hypothesized that this different spatial distribution between the two cellular strains could reflect the different metabolic activity of LoVo-R cells respect to their sensitive counterpart. Considering the well known role of $MgATP^{2-}$ in buffering Mg^{2+} intracellular content, it has been postulated that the levels of Mg^{2+} binded to ATP represent a key parameter in regulation of protein synthesis and cell proliferation leading to neoplastic transformation.[88] Moreover, efflux pumps characterizing the MDR phenotype, belong to ATP binding cassette protein family and need energy to function; in this scenario it has to be consider that Mg^{2+}-ATP^{2-} is the only active form of ATP. Therefore higher intracellular Mg^{2+} concentration is coherent with the idea that an increase energy demand is required to potentiate mitochondrial energetic function and consequently the activity of efflux pumps, which are highly dependent from ATP.[103]

Subsequently, combining volumetric information obtained by AFM measurements with STXM we calculate Mg^{2+} molar concentration of dehydrated cells.

As shown in figure 28, in a population of 14 LoVo-S cells and 13 LoVo-R single cells, different distribution of Mg^{2+} concentration values were detected. The amount of total intracellular Magnesium has been calculated to be 55±27 mM and 88±38mM for the two strains respectively. It is worth noting that trend of Mg^{2+} concentration found in single cell population is of the same order of magnitude to that previously found in large cell population with DCHQ5 assay.

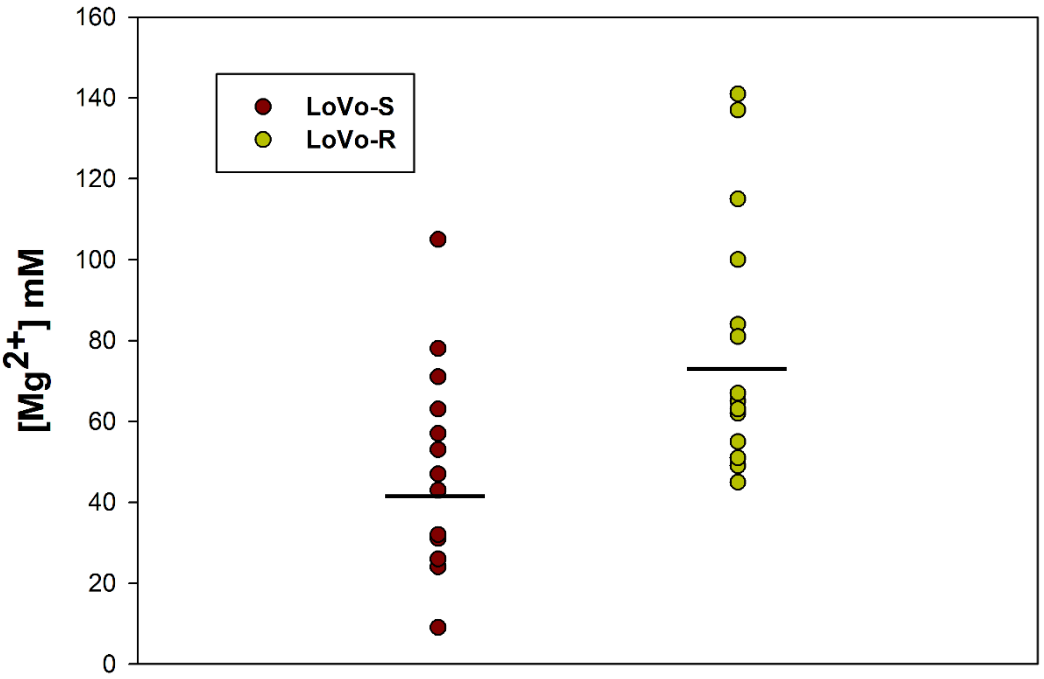

Figure 28 Single cell population analysis of Total Mg concentrations in LoVo-S and Lovo-R cells. Magnesium intracellular concentration was evaluated by synchrotron radiation referring to volume of dehydrated cells previously calculated by AFM. The black bar represent mean channel value.

Although, we used cryogenic methods of fixation to preserve the chemical integrity of the cell and its morphology, this method of fixation as well as all the other available methods, presents the inconvenience of reducing cellular volume. The decrement of cellular volume can be attributed to the loss of H_2O inside the cells.

Therefore, aimed to reach the exact value of molar concentration in our fixed cells we decided to refer the total amount of Mg^{2+} found in single dehydrated cells to the volume of hydrated cells calculated by Beckman Coulter Counter (see figure 25). Histograms reported in figure 29, displays the comparison

between large cell population data and single cells data of the Mg^{2+} intracellular concentration found both in sensitive (purple) and resistant (green) cells. It is worth underlining that single cells data are almost overlapping those obtained in large cell population.

It is confirmed that LoVo-R cells show a relevant increase of Mg^{2+} concentration compared to LoVo-S.

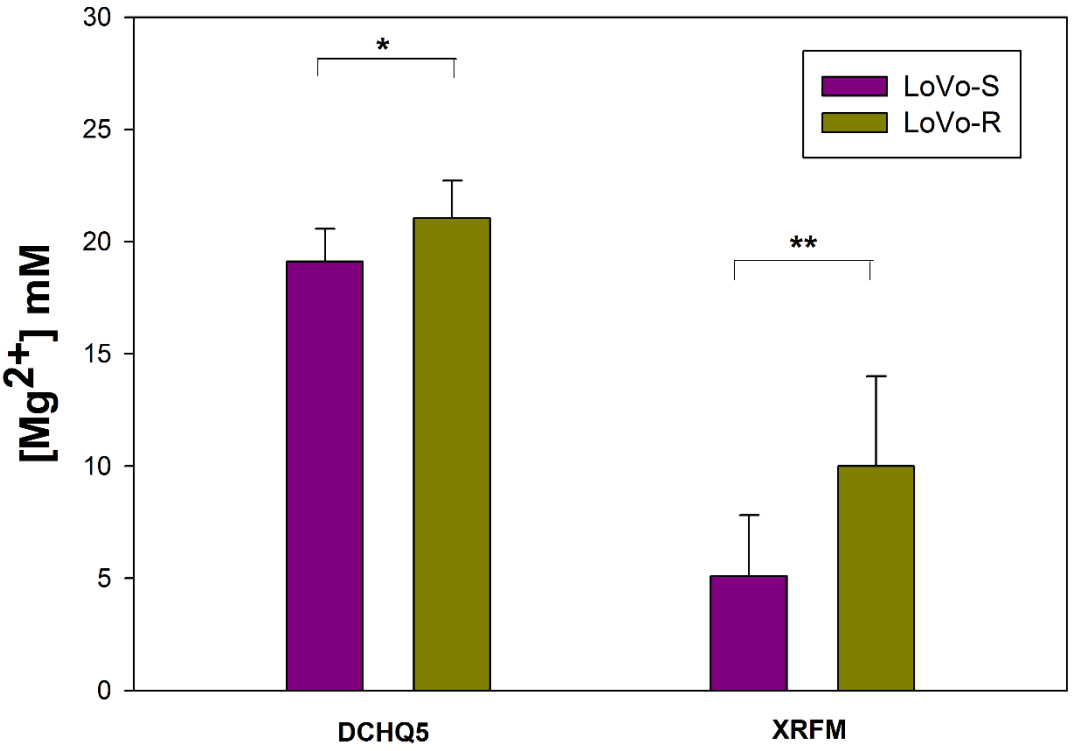

Figure 29 Comparison of Total Mg^{2+} concentrations in LoVo-S and Lovo-R cells assessed by two different techniques: DCHQ5 spectrofluorimetric assay and XRFM multimodal approach. Magnesium intracellular concentration was evaluated by DCHQ5 fluorescence and synchrotron radiation referring to volume of hydrated cells.* P~0.02 ** P<0.01

6 Conclusions

Magnesium is a critical cofactor of many enzymatic reactions important for physiological functions, such as nucleic acid metabolism, protein synthesis and energy production. Growing evidences point to a possible role for this cation in the apoptotic process but the available literature is still scarce and contradictory. Nevertheless, both intrinsic and extrinsic pathways of apoptosis are accompanied by variations in cytosolic magnesium, and magnesium appears to be required for the release of cytochrome *c* from isolated mitochondria. Given the central role of mitochondria in apoptosis, their ion channels are emerging as promising targets for cancer treatment. As a consequence of changes in ion flux across the inner mitochondrial membrane, alterations of mitochondrial function occur that produce severe effects on the overall health, including ATP production, of these organelles.[138] In this regard, the presence of a Mg^{2+} selective influx channel in mitochondria (MRS2) suffrages the hypothesis of the involvement of magnesium in the apoptotic onset.

The study herein reported is the first on the effect of regulated expression of mitochondrial Mg^{2+} channel MRS2 on induced apoptotic cells.

Clones derived from HEK-293 cell line, died within a few hours after inducing apoptosis, as revealed by cell cycle analysis, nuclear condensation, DNA fragmentation and cleavage of cysteinyl proteases. On the contrary, cells overexpressing MRS2 protein were more resistant to all the apoptotic stimuli performed.

The underlying mechanism of this effect may still relate to the role of MRS2 protein in the regulation of mitochondrial functions. The concept of a possible network between drug sensitivity and mitochondrial function, morphology and

or localization is not conceptually new. Mitochondria are known to take active part in the apoptotic process by various mechanisms including release of caspase activators, disruption of electron transport and energy metabolism, and production of reactive oxygen species. In conclusion, the fact that activation of the mitochondrial death pathway represents the major mechanism of most conventional anticancer drugs, including DXR and STS, could explain why cells overexpressing MRS2 channel overcome the induced apoptosis.

However it has to be point out that cell cycle progression of cells overexpressing MRS2 and treated with STS appeared to be more affected by the drug compared with DXR treatment, this could due to the possibility to the triggering of a different apoptotic pathway independent from caspases activation.[151]

Further investigations are needed to evaluate the biological role of Mg^{2+} in resistance to anticancer drugs by promoting the cells to overcome apoptosis signal.

Moreover, we showed for the first time that overexpression of mitochondrial Mg^{2+} influx channel MRS2 induces an increment of total intracellular Mg^{2+}. However, recent findings report a new mitochondrial magnesium transporter in yeast, the Mme1 protein that seems to act as a magnesium exporter.[152] In this contest, it will represent a challenging task to investigate whether this export mechanism is also expressed in our experimental model.

Obviously, these findings open a multitude of questions upon the functional implications of MRS2 protein in Mg^{2+} perturbation associated diseases..

In the second part of this research, we studied Mg^{2+} distribution and concentration in MDR cell model together with the possibility to give new insight into Mg^{2+} quantification.

The main goal of the research was to verify whether magnesium intracellular content and compartmentalization could be used as a signature to distinguish MDR tumour cells from their drug-sensitive counterparts.

Single cell population analysis, performed by a new multiparametric approach revealed a different patterns in the maps of Mg^{2+} concentration of the two cellular strains. In particular, LoVo-R cells present higher values within the nucleus in and in the perinuclear region respect to LoVo-S cells.

Interestingly, perinuclear region of the cells is very rich in mitochondria organelles. The mitochondria located in this area form a barrier, named perinuclear mitochondria, for which it has been hypothezed a protecting role in defending nucleus against invasion of intracellular Ca^{2+} signals[153].

On these bases, the implication of this different distribution of Mg^{2+} in MDR cells could be related to the regulation of the energetics of nuclear transport and in triggering release of activators of apoptosis from perinuclear mitochondria.

Furthermore, live cells loaded with DCHQ5 chemosensor showed higher Mg^{2+} levels in LoVo resistance colon cancer cells. This result was then confirmed, quantifying intracellular Mg^{2+} by DCHQ5 chemosensor in sonicated large cell population finding higher Mg^{2+} concentration in LoVo-R cells respect to LoVo-S. This latter result is coherently with that obtained by XRFM-AFM analysis in whole single cells revealing higher Mg^{2+} concentration in cells presenting MDR phenotype.

It must be emphasized that, although the approaches used to quantify Mg^{2+} intracellular concentration were profoundly different, the average intracellular Mg^{2+} concentration found in a population of 10^5 cells assessed by DCHQ5-assisted fluorimetric assay is of the same order of magnitude of that found in a sample of about 27 single cells by XRFM-AFM analysis. This is not a trivial result, since recent studies on single-cell analysis drew attention to the problem of cell heterogeneity in large population. To this extent, a very recent study

showed a difference of two orders of magnitude in the concentration of intracellular TiO2-nanoparticles assessed in single cells or in cell population.[154] This feature open a new scenario in the significance of Mg^{2+} in cancer and in characteristic of cells developed MDR phenotype.

REFERENCES

[1] M. E. Maguire, J. A. Cowan. *Biometals* 2002, 15:203-210;

[2] M. A. Shand *The Chemistry and Technology of Magnesia* John Wiley & Sons,2006, 266;

[3] Y. Nishizawa, H. Morii, J. Durlach *New Perspectives in Magnesium Research. Nutrition and Health.* 2007 Springer-Verlag London;

[4] H Davy.*Philos. Trans. R. Soc. Lond.* 1808, 98: 333–370;

[5] J.H. De Baaij, JG Hoenderop, Bindels RJ. *Physiol. Rev*., 2015, 95:1-46;

[6] A. Sgambato, F.I. Wolf, B. Faraglia, A. Cittadini, J. *Cell. Physiol*., 1999, 180:245–254 ;

[7] P. Chellan, P.J. Sadler, 2015 *Philos. Trans. A. Math. Phys. Eng. Sci*. 2015 13:373-;

[8] Institute of Medicine (IOM). *Food and Nutrition Board. Dietary Reference Intakes: Calcium, Phosphorus, Magnesium, Vitamin D and Fluorideexternal link icon*. Washington, 1997, DC: National Academy Press;

[9] Y. Song, J.E. Manson, J.E. Buring, S. Liu *Diabetes Care* 2004,27: 59–65;

[10] N.M. Ramadan, H. Halvorson, A. Vande-Linde, S.R. Levine, .JA. Helpern, K.M. Welch, *Headache* 1989, 29: 590–593;

[11] A. Romani. A. Scarpa, *Arch. Biochem. Biophys*. 1992, 298:1-12;

[12] F. I. Wolf, A. Torsello, S. Fasanella, A. Cittadini. *Mol. Aspects Med*. 2003, 24:11-26;

[13] F. I. Wolf, A. Cittadini. *Mol. Asp. Med.* 2003, 24:3-9;

[14] M. Fatholahi, K. Lanoue, A. Romani, A. Scarpa. *Arch. Biochem. Biophys*. 2000, 374:395- 401;

[15] T. Kubota, Y. Shindo, K. Tokuno, H. Komatsu, H. Ogawa, S. Kudo, Y. Kitamura, K. Suzuki, K. Oka. *Biochim. Biophys. Acta* 2005, 1774:19-28;

[16] R.M.Touyz, *Am.J.Physiol.Heart Circ.Physiol.* 2008, 294:H1103-H1118;

[17] A.M.P. Romani. *Met. Ions Life Sci*. 2013, 12:69-118;

[18]M. Kolisek, R.J. Schweyen,M.Schweige, *New Perspectives in Magnesium Research and Health*, Chapter 3,2007,Springer-Verlag London;

[19] S. Iotti, C. Frassineti, L. Alderighi, A. Sabatini, A. Vacca, B. Barbiroli. *NMR Biomed.* 1996; 9 24-32;

[20] H. Ebel, T. Gunther *J Clin. Chem. Clin. Biochem.* 1980, 18: 257–270;

[21] T. Kubota, Y. Shindo, K. Tokuno, H. Komatsu, H. Ogawa, S. Kudo, Y. Kitamura, K. Suzuki, K. Oka. *Biochim. Biophys. Acta*, 2005, 1774:19-28;

[22] G. Farruggia, S. Iotti, L. Prodi, N. Zaccheroni, M. Montalti, P. B. Savage, V. Trapani, P. Sale, F. I. Wolf. *J. Am. Chem. Soc*. 2006, 128:344-350;

[23] A. Romani, E. Dowell, A. Scarpa, *J. Biol. Chem.* 1991 266:24376–24384;

[24] G.H. Zhang, J.E. Melvin, *J. Biol. Chem*. 1996, 271:29067–29072;

[25] A. Romani. *Arch. Biochem. Biophys*. 2011, 512:1-23;

[26] D.G. Kehres, C.H. Lawyer, M.E. Maguire *Microb. Comp. Genomics* 1998, 3:151–159;

[27] M.B. Moncrief, M.E. Maguire *J. Biol. Inorg. Chem.* 1999, 4:523–527;

[28] R.R. Preston *Science,* 1990, 250: 285–288.

[29] J. Payandeh , EF Pai *EMBO J.*2006, 25:3762-73;

[30] J. A. Cowan *Biometals* 2002,15:225 – 235;

[31]J. Payandeha, R. Pfohb, EF. Pai, *Biochim. Biophys. Acta– Biomembr.* 2013, 1828,1828: 2778–2792;

[32] D. Niegowski, S. Eshaghi, *Cell. Mol. Life Sci.* 2007,64:2564–2574;

[33]T. Gunther, J. Vorman.R.Forster, *Biochem. Biophys. Res. Commun.* 1984, 119:124-131;

[34] C. Cefaratti, C. Ruse, *Mol. Cell. Biochem.* 2007,297:209–214;

[35] H .Ebel, M. Hollstein, T. Gunther *Biochim. Biophys. Acta 2002,1559:135-144;*

[36] G. J Liu, D. K.Martin, R.C. Gardner,P.R. Ryan FEMS *Microbiol. Lett* 2002,. 213: 231 – 237;

[37] A Graschopf, R. J. Schweyen, *J. Biol. Chem.* 2001, 276:16216–16222;

[38] G. Zsurka,J.Gregan, R.j.Schweyen 2001 *Genomics,* 72:158-168;

[39] H. Zhou, D.E. Clapham, *Proc. Natl. Acad. Sci.* 2009, 106:15750–15755.

[40] M.B.Khan, G.Sponder, B.Sjoblom, S.Svidova, R.j.Schweyen, O.Carugo, K.D.Carugo, *Acta Cryst.* 2013,69:1653-1664;

[41] D.M. Bui, J. Gregan, E. Jarosch, A. Ragnini, R.J. Schweyen, 1999 *J. Biol. Chem.* 274:20438–20443;

[42] M. Kolisek, G. Zsurka, J. Samai. J. Weghuber, R. J. Schweyen, M. Schweigel. *EMBO J*. 2003, 22:20438-20443;

[43] S. Assou, et al. *BMC Genomics*, 2009,10:1-10;

[44] A.J. Worlock, R.L.Smith *J. Bacteriol*. 2002,184:4369-4373;

[45] Y. Chen, X. Wei, P. Yan, Y. Han, S. Sun, K .Wu, D. Fan. *Cancer Biol. Ther.* 2009,8:607-614 ;

[46] M. Piskacek, L. Zotova, G. Zsurka, R.J. Schweyen *J. Cell. Mol. Med*., 2009, 13:693–700;

[47] Y. Zhao, H. You, F. Liu, H. An, Y. Shi, Q. Yu, D. Fan *Cancer Lett.* 2002; 185:211-218;

[48] S. McNulty, E. Fonfria, *Europ. J. Physiol.*2005,451:235-241;

[49] K.P. Schlingmann, S. Weber, M. Peters, L. Niemann Nejsum, H. Vitzthum, K. Klingel, M. Kratz, E. Haddad, E. Ristoff, D.Dinour M. Syrrou, S. Nielsen, M. Sassen, S. Waldegger, H.W. Seyberth, M. Konrad *Nature Genet.* 2002, 31:166–170;

[50] M.J. Nadler, M.C. Hermosura, K. Inabe, A.-L. Perraud, Q. Zhu, A.J. Stokes, T. Kurosaki, J.P. Kinet, R. Penner, A.M. Scharenberg, A. Fleig, *Nature* 2001, 411:590–595;

[51] L. V. Ryazanova, Z. Hu, S. Suzuki, V. Chubanov, A. Fleig, A.G. Ryazanov *Scient. Rep.* 4, Art. Numb.: 7599 doi:10.1038/srep07599;

[52] I. Dhennin-Duthille, M. Gautier, I. Korichneva, H. Ouadid-Ahidouch, *Magnes. Res*. 2014, 27:103-12;

[53] D.B. Simon, Y. Lu, K.A. Choate, H. Velazquez, E. Al-Sabban, M. Praga, G. Casari, A. Bettinelli, G. Colussi, J. Rodriguez-Soriano, D. McCredie, D. Milford, S. Sanjad, R.P. Lifton *Science* 1999, 285: 103–106;

[54] A. Goytain, G. A. Quamme. *BMC Geomics* 2005, 6:48;

[55] I. Dhennin-Duthille, M. Gautier, I. Korichneva, H. Ouadid-Ahidouch, *Magnes. Res*. 2014, 27:103-12;

[56] J. Sahni, A.M. Scharenberg *Mol. Med. Aspects* 2013, 34:620–628;

[57] M. Kolisek, P. Launay, A. Beck, G. Sponder, N. Serafini, M. Brenkus, E.M. Froschauer, H. Martens, A. Fleig, M. Schweigel *J Biol. Chem*. 2008, 283:16235-47;

[58] A. Tucci, M.A. Nalls, H. Houlden, T. Revesz, A.B. Singleton, N.W. Wood, J. Hardy , C. Paisan-Ruiz. *Eur. J Hum. Genet*. 2010, 18:1356–1359;

[59] S. Hardy, N. Uetani, N. Wong, E. Kostantin, D.P. Labbe, L.R. Begin, A. Mes-Masson , D. Miranda-Saavedra, M.L.Tremblay *Oncogene* 2014, doi:10.1038/onc.2014.33;

[60]T. Günther, V. Höllriegl, *Biochim. Biophys. Act*a 1993, 1149 :49–54.

[61] A. Romani, A. Scarpa, *Nature* 1990, 346:841–844;

[62] J. Vormann, T. Gunther, *Magnesium,*1987, 6:220–224.

[63] A. Jakob, J. Becker, G. Schottli, G. Fritzsch, *FEBS Lett*. 1989, 246:127–130;

[64] V. Gaussin, P. Gailly, J.-M. Gillis, L. Hue, *Biochem. J.* 1997, 326:823–827;

[65] J. J. Erdos, M. E. Maguire. *J. Physiol*. 1983, 337:351-371;

[66] T. Günther, J. Vormann, *Biochim. Biophys. Acta* 1995, 1234:105–110;

[67] R. M. Touyz, G. Yao. *J. Cell. Physiol*. 2003, 197:326-335;

[68] S. Thebault, R. T. Alexander, W. M. Tiel Groenstege, J. G. Hoenderop, R. J. Bindels. *J. Am. Soc. Nephrol*. 2009, 20:78-85;

[69] E.S. Ford, A.H. Mokdad. *J Nutr.* 2003, 133: 2879–2882;

[70] F. Heaton , L. Pyrah , C. Beresford, R. Bryson, D. Martin *Lancet* 1962280: 802–805;

[71] M. Stuiver, S. Lainez, C. Will, S. Terryn, D. Gunzel, H. Debaix, K. Sommer, K. Kopplin, J. Thumfart, N.B. Kampik, U. Querfeld, T.E. Willnow, V. Nemec, C.A. Wagner, J.G. Hoenderop, O. Devuyst, N.V. Knoers, R.J. Bindels, I.C. Meij, D. Muller. *Am J Hum Genet* 2011, 88: 333–343;

[72] S. Tejpar, H. Piessevaux, K. Claes, P. Piront, J.G.J. Hoenderop, C. Verslype, E. Van Cutsem *Lancet Oncol* 2007, 8: 387–94;

[73] Z. Erdtman,. *Physiol. Chem*. 1927,172-182 ;

[74] U. Blaszczyk, A. Duda Codach *Rocz Panstw Zakl Hig* 2013, 64:165-171;

[75] W.E.C. Wacker *Pathogenesis and Clinical Significance of Magnesium Deficiency* 1969, 162:717–726;

[76] L.Garfinkel, D. Garfinkel *Magnesium* 1985, 4: 60–72;

[77] A. Romani. *Arch. Biochem. Biophys*. 2007, 458:90-102;

[78] J. Anastassopoulou, T. Theophanides *Crit. Rev. Oncol. Hematol* 2002, 42: 79–91;

[79] A.Hartwig. *Mutat. Res*. 2001, 475:113–121;

[80] L.T. Iseri, J.H. French *J Am. Heart.* 1984,108:188–193;

[81] F.Y. Li, B. Chaigne-Delalande, C. Kanellopoulou, J.C. Davis, H.F. Matthews, D.C. Douek, J.I. Cohen, G. Uzel, H.C. Su, M.J. Lenardo. *Nature* 2011, 475: 471–476;

[82] F.I.Wolf, F.Trapani, A.Cittadini *Magnes. Res*.2008, 21 (2): 83-91;

[83] F.I. Wolf, S. Fasanella, B. Tedesco, A. Torsello, A. Sgambato, B. Faraglia, P. Palozza, A. Boninsegna, A. Cittadini *Front Biosci* 2004, 9: 2056-2062;

[84] A. Sgambato, F.I. Wolf, B. Faraglia, A. Cittadini, *J. Cell. Physiol*. 1999, 180:245–254;

[85] V. Covacci, N. Bruzzese, A. Sgambato, A. Di Francesco, M.A. Russo, F.I. Wolf, A. Cittadini, *J. Cell. Biochem*. 1998, 70:313–322;

[86] R.M.Touyz, G.Yao *J Cell Physiol*. 2003, 197:326-335;

[87] F.I. Wolf, V. Trapani, *Clin. Sci*. 2008, 114, 27–35;

[88] H. Rubin. *Adv. Cancer Res*. 2005, 93:1-58;

[89] C. Cappadone, L. Merolle, C. Marraccini, G.Farruggia, A.Sargenti,A. Locatelli, R.Morigi, S.Iotti *Magnes.Res*. 2012, 25:104-11;

[90] A. Andreani, M. Granaiola, A. Locatelli, R. Morigi, M. Rambaldi, L. Varoli, N. Calonghi, C. Cappadone, G. Farruggia, C. Stefanelli, L. Masotti, T.L. Nguyen, E. Hamel, R.H. Shoemaker. *J Med. Chem.* 2012, 55:2078-88;

[91] L. Merolle, C. Cappadone,G Farruggia, C.Marraccini, A Sargenti, A Colanardi, S. Iotti *J. Biol. Res.* 2014; 87:2139-2143;

[92] J. Li, W. Li, W. Liu, B.T. Altura, B.M. Altura *Drug Metab Lett* 2007, 1: 85-89;

[93] C. Malpuech-Brugère, W. Nowacki, M. Daveau, E. Gueux, C. Linard, E. Rock, J. Lebreton, A. Mazur, Y. Rayssiguier *Biochim Biophys Acta*. 2000 15;150:91-98;

[94] T. Patel, S.F. Bronk, G.J. Gores *J Clin. Invest*. 1994, 94:2183-92;

[95] R. Eskes, S. Desagher, B. Antonsson, J.C. Martinou *Mol Cell Biol*. 2000, 2: 929–935;

[96] I. Solaroglu, E. Kaptanoglu, O. Okutan, E. Beskonakli, A. Attar, K. Kilinc *Surg. Neurol* 2005, 64 Suppl 2:S17-21;

[97] C. Türkyilmaza, Z. Türkyilmazb, Y. Atalaya, F. Söylemezogluc, B. Celasund *Brain Res*.2002, 955:133–137

[98] S. Ravishankar, Q.M. Ashraf, K. Fritz, Om P. Mishra, M. Delivoria-Papadopoulos *Brain Research* 2001,901:23-29;

[99] F.I. Wolf, J.A.M. Maier, A. Nasulewicz, C. Feillet-Coudrayd, M. Simonaccia, A. Mazur, A. Cittadini *Arch.Biochem.Biophys*. 2007,458: 24–32;

[100] A. Wang, N. Yoshimi, T. Tanaka, H .Mori *Canc. Lett.* 1993, 75: 73–78;

[101] A. Nasulewicz, J. Wietrzyk, F.I. Wolf, S. Dzimira, J. Madej, J.A. Maier, Y. Rayssiguier, A. Mazur, A. Opolski *Biochim Biophys Acta*. 2004, 1739:26-32;

[102] F.I. Wolf, A.R.M. Cittadini, J.A.M. Maier *Cancer Treat. Rev*., 2009 35:378-382;

[103] F. I. Wolf, V. Trapani *Clin. Sci.* 2012, 123:417–427;

[104] B. Vincenzi, D. Santini, S.Galluzzo, A.Russo, F.Fulfaro, M.Silletta, F.Battistoni, L.Rocci, B.Beomonte Zobel, V.Adamo, G.Dicuonzo, G.Tonini *Clin.Canc. Res.* 2008,14:4219-4224;

[105] R. Krishna, L. D Mayer *Eur J Pharm Sci.* 2000 11:265-283;

[106] A. Bisi, S. Gobbi, L. Merolle, G. Farruggia, F. Belluti, A. Rampa, J. Molnar, E. Malucelli, C. Cappadone Eur *J Med. Chem*. 2015, 92:471-480;

[107] W. Szaflarskia, P. Sujka-Kordowskaa, R. Januchowskia, K. Wojtowicza, M. Andrzejewskaa, M. Nowickia, M. Zabela *Biomed. Pharmacother*.2013,67:497-502;

[108] H. Lage, *Cell. Mol. Life Sci*. 2008, 65:3145–3167;

[109] S.H. Kaufman, W.C. Earnshaw *Exp. Cell Res.* 2000, 256: 42–49;

[110] J. Plati, O. Bucur, R. Khosravi-Far *Integ Biolm* 2011, 3: 279-96;

[111] F. I. Wolf, V. Trapani *Cancer Biol.Ther*. 2009, 8:615-617;

[112] G. Marverti, A. Ligabue, M. Montanari, D. Guerrieri, M. Cusumano, M.L. Di Pietro, L. Troiano, E. Di Vono, S. Iotti, G. Farruggia, F.I. Wolf, M.G. Monti, C. Frassineti *Invest. New Drugs* 2011, 29:73-86;

[113] A. Sargenti, G. Farruggia, E. Malucelli, C. Cappadone, L. Merolle, C. Marraccini, G. Andreani, L. Prodi, N. Zaccheroni, M. Sgarzi, C. Trombini, M. Lombardo S. Iotti *Analyst* 2014, 139:1201-1207;

[114] V. Trapani, G. Farruggia, C. Marraccini, S.Iotti, A. Cittadini, F.I.Wolf *Analyst* 2010, 135:1855-1866;

[115] L.H. Lindenburg, J.L. Vinkenborg, J. Oortwijn, S.J,A.Aper, M. Merks, *PLoS ONE* 2013, 8: e82009

[116] C.Yu, Q. Fu, J. Zhang, *Sensors (Basel)*2014, 14: 12560–12567;

[117] L. A. Levy, E. Murphy, B. Raju, R. E. London *Biochemistry* 1988, 27:4041–8;

[118] B. Raju, E. Murphy, L. A. Levy, R. D. Hall, R. E. London *Am. J. Physiol*.1989, 256:C540–C548;

[119] H. M. Kim, C. Jung, B. R. Kim, S. Y. Jung, J. H. Hong, Y. G. Ko, K. J. Lee and B. R. Cho, *Angew. Chem., Int. Edit.* 2007, 46:3460;

[120] C. Marraccini, G. Farruggia, M. Lombardo, L. Prodi, M. Sgarzi, V. Trapani, C. Trombini, F. I. Wolf, N. Zaccheroni, S. Iotti. *Chem. Sci.,* 2012, 3:727-734;

[121] Y. Shindo, T. Fujii, H. Komatsu, D. Citterio, K. Hotta, K. Suzuki, K. Oka. *PLosOne* 2011, 6:8 e23684;

[122] H. Laurens, J. Lindenburg, L.Vinkenborg., Jorn Oortwijn, S. J. A. Aper, M.Merkx *PLosOne*8 2013, (12): e82009;

[123] S. Lagomarsino, S. Iotti, G. Farruggia, A. Cedola, V. Trapani, M. Fratini, I. Bukreeva, A. Notargiacomo, L. Mastrototaro, C. Marraccini, A. Sorrentino, I. McNulty, S. Vogt, D. Legnini, S. Kim, A. Gianoncelli, J. A. M. Maier, F. I. Wolf. *Spectrochim. Acta Part B:Atomic Spectroscopy* 2011, 66:834-840

[124] S. J. B. Reed, 2005, *Electron Microprobe Analysis and Scanning Electron Microscopy in Geology (2nd Ed.)*, Cambridge University Press;

[125] S. Roudeau ,A. Carmona, L.Perrin ,R. Ortega *Anal. Bioanal. Chem.* 2014, DOI 10.1007/s00216-014-8004-8014;

[126] E. Malucelli, S.Iotti, A. Gianoncelli, M. Fratini, L. Merolle, A. Notargiacomo, C. Marraccini, A. Sargenti, C. Cappadone, G. Farruggia . I.Bukreeva , M. Lombardo , C. Trombini, J. A. Maier , S. Lagomarsino *Anal. Chem* 2014, 86:5108–5115;

[127] R.S.Y. Wong g *J Exp. & Clin. Canc. Res.* 2011, 30:87;

[128] J.F. Kerr, B.V. Harmon *Definition and incidence of apoptosis: an historical perspective. In Apoptosis: the molecular basis of cell death.* Vol. Tomei LD, Cope FO. New York: *Cold Spring Harbor Laboratory Press* 1999, 5-29;

[129] J.F Kerr, A.H. Wyllie, A.R. Currie *Br. J. Cancer* 1972, 26: 239–257;

[130] T.T. Reanult, E.J. Chipuk *J Biol. Chem.* 2014, 289:26481-26491;

[131] C.M. Walsh *Front. Cell. Dev. Biol.* 2014, 2:3;

[132] J. Plati, O. Bucur, R. Khosravi-Far *Integr Biol (Camb).* 2011;3:279-96;

[133] L. A. Gillies, T. Kuwana *J Cell. Biochem.* 2014, 115: 632-640;

[134] R. Elkholi, K.V.Floros, J.E. Chipuk *Genes Cancer* 2011, 2:523–37;

[135] E. Devarajan, A.A. Sahin, J.S. Chen, R.R. Krishnamurthy, N. Aggarwal, A.M. Brun, A. Sapino, F. Zhang, D. Sharma, X.H. Yang, A.D. Tora, K. Mehta *Oncogene* 2002, 21:8843-8851;

[136] R. Ferraresi, L. Troiano , M. Pinti, E. Roat, E. Lugli, D. Quaglino, D. Taverna, D. Bellizzi, G. Passarino, A. Cossarizza *Cytometry* 2008 ,73:528-537;

[137] S. H.Kaufmann, W. C. Earnshaw *Exp. Cell Res.* 2000, 256:42-49;

[138] L. Leanza, M. Zoratti, E. Gulbins , I. Szabo *Oncogene* 2014, 1–13;

[139] F. I. Wolf, V. Trapani *Cancer Biol Ther*., 2009 8:615-617;

[140] K. Postle, T.T. Nguyen, K. P. Bertrand *Nucleic Acids Res.* 1984, *12*: 4849-4863;

[141] W.Hillen, C. Berens, *Annual Rev.in Microbiol.* 1994, 48:345-369;

[142] J. Graham *The Scientific World Journal* 2002, 2:1638-1642;

[143] I. Stanic, A. Facchini, R.M. Borzì, C. Stefanelli, F. Flamigni *J. Cell Physiol.* 2009, 219: 109–116;

[144] F.L. Graham *J. Gen. Virol*. 1977, 36: 59-72;

[145] I. Assanga, L. Lujan *Int. J Biotech. Mol. Biol.Res.* 2013, 4:, 60-70;

[146] M. Torkzadeh-Mahani, F. Ataei, M. Nikkhah, S. Hosseinkhani *Biosens. Bioelectron.* 2012 38:362-368;

[147] A.P. Trapé, M.L. H Katayama, R.A. Roela, H. Brentani, G.R. Ravacci, L. de Araujo Lima, M. M Brentani *Mol. Canc. Ther.*, 2012. 11:464-474;

[148] A. Antonsson, J.L. Persson, *Anticancer Res.* 2009, 29:2893-2898;

[149] M. Barbagallo, M. Belvedere, G. Di Bella, L.J. Dominguez *Magnes.Res.*2011, 24: 115-121;

[150] C. Marraccini, G. Farruggia, M. Lombardo, L. Prodi, M. Sgarzi, V. Trapani, C. Trombini, F. I. Wolf, N. Zaccheroni, S. Iotti *Chem. Sci.* 2012, 3:727-734;

[151] C.A. Belmokhtar, J. Hillion, E. Ségal-Bendirdjian *Oncogene* 2001, 20:3354-3362;

[152] Y.Cui, , S.Zhao, J. Wang, X. Wang, B. Gao,Q. Fan,B. Zhou *Biochim. Biophys. Acta (BBA)-Mol. Cell Res.* 2015;

[153] M. Kyu Park, M. C. Ashby, G. Erdemli, O.H. Petersen, A.V. Tepikin *EMBO J*. 2001, 20 1863–1874;

[154] J.T. Rashkow, S.C. Patel, R. Tappero, B. Sitharaman *R. Soc. Interf.* 2014, 11:94, 20131152.